A Study on Ion/Molecule Reactions of Silver Cluster Cations with Crown Ethers using an Ion Trap Time-of-Flight Mass Spectrometer

（イオントラップ飛行時間型質量分析計による
銀クラスターカチオンとクラウンエーテルの
イオン／分子反応の研究）

Kousuke Kumondai

Department of Physics, Graduate School of Science,
Osaka University

March, 2004

Abstract

Crown ethers exhibit binding abilities with metal cations and size-dependent efficiencies of complex formation. These reactions have become important for understanding basic process of molecular recognition. For alkali metal cations, many investigations on these reaction processes have been performed. However, these reactions of metal cluster cations have not been reported. Clusters have complex geometrical structures and their sizes are larger than those of atom cations. Therefore, the ion/molecule reactions of metal cluster cations with crown ethers are interesting topics of physical chemistry. This thesis consists of the three following subjects:

- For observing gas-phase ion/molecule reactions of metal clusters, a cylindrical ion trap time-of-flight mass spectrometer was newly constructed. This apparatus consists of an external sputtering ion source, deceleration lens system, cylindrical ion trap and a time-of-flight mass analyzer with four toroidal electric sectors. The technical data for construction and the results of the tests for checking the performance were reported.

- Using this apparatus, ion/molecule reactions of alkali metal cations (K^+, Rb^+ and Cs^+) with crown ether were observed. Observed reactions were similar to those reported previously. The reaction rate constants of each reaction were determined. Comparing these values with those reported previously, it was confirmed that this apparatus can be used for obtaining relative rate constants.

- Ion/molecule reactions of silver cluster cations, Ag_n^+ (n = 1, 3, 5, 7 and 9), with crown ether were observed for the first time. In case of Ag^+, the reactions that are similar to alkali metal cations occurred. In case of Ag_3^+, formations of 1:1, 1:2, 3:1, 3:2 and 3:3 complexes were observed. In case of Ag_5^+, various reaction products such as 1:2, 3:3, 5:3, etc. were observed. In case of Ag_7^+ and Ag_9^+, 1:2 complex was observed as the major products. These reactions might be attributable to the electronic structure of Ag_5^+. The results suggest that the the dissociation of Ag_3^+ and Ag_2 from Ag_5^+ is favorable process because both Ag_3^+ and Ag_2 correspond to the magic numbers.

Contents

Chapter 1

Introduction

Macrocyclic polyethers (crown ethers), discovered by Pedersen [1] in 1967. It is known that crown ethers exhibit binding abilities with metal cations and efficiencies of reactions depend on the size of cations. These reactions have become important for understanding molecular recognition, which is based on size- or shape- specific interactions between molecules. Especially, these reactions in the gas-phase are important because they provide fundamental informations without effects arising from solvent or counterions. Thus many investigations on gas-phase reactions of metal cations with crown ether have been performed [2, 3, 4, 5].

Crown ethers are expressed by the composition formula as c-$(C_2H_4O)_n$. By usage, they are called "$3n$-crown-n," where "$3n$" and "n" indicate the total number of atoms composing the ring and the number of oxygen atoms contained in the molecule. For typical examples, schematic geometries of crown ethers, c-$(C_2H_4O)_4$ (12-crown-4) and c-$(C_2H_4O)_5$ (15-crown-5) are shown in Fig.1.1. As shown in the figure, crown ethers have cavities. Cations are strongly bound in the

cavity because the oxygen atoms in the ring structure are charged negative. Then cations and crown ethers form metal-ligand complexes. Metal-ligand complexes also undergo reaction with a second ligand to form 1:2 metal-ligand complexes, which are called "sandwiches." Chu et al. [6] have reported that the efficiencies of 1:1 complexation and sandwich formation of alkali metal cations are strongly dependent on the cation charge density and the ratio of cation radius to binding cavity radius, respectively. For example, the efficiencies of 1:1 complex formation are generally $Na^+ > K^+ > Rb^+ > Cs^+$. These size-specific reactions of various cations are of interest. However, reactions of clusters, which can be regarded as "large molecules," with crown ethers have not been investigated yet. Therefore, the investigations on these reactions can provide new informations such as reaction pathways and products. These informations give basic knowledge of chemistry and physics.

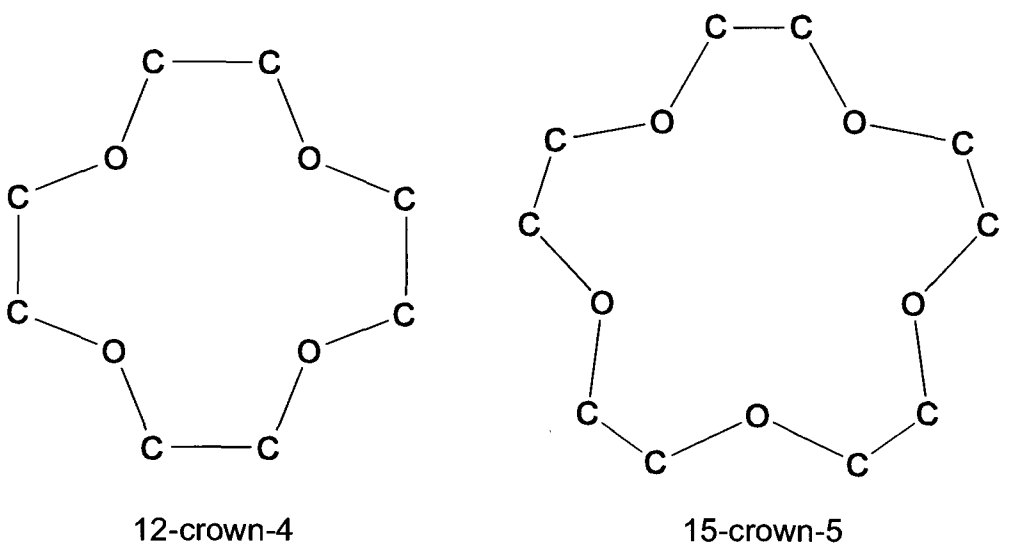

Figure 1.1: Schematic geometries of 12-crown-4 (left) and 15-crown-5 (right). The signs of hydrogen (H) are abbreviated.

Cluster is an aggregate consisting of 2–1000 atoms or molecules. One of the most characteristic points of the cluster is that most of containing atoms are exposed on the surface. Cluster is thought as an intermediate phase between an atom and bulk state as shown in Fig.1.2. It shows peculiar physical and chemical properties such as its stabilities, chemical reactions, catalyst actions, and so on. The explosion of growth in studies on clusters has been phenomenal over the past 20 years.

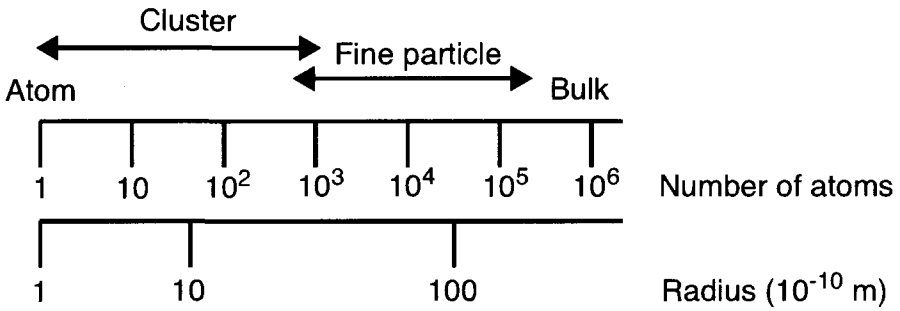

Figure 1.2: Phase-classification of material according to the number of the particles.

The stabilities, structures and other properties of the clusters strongly depend on their size (number of consisting atoms). For example, the discontinuous variations in the intensities are often observed in their mass spectra. These anomalous sizes of the cluster are called "magic numbers." Therefore, mass spectrometers, which can separate the cluster ions according to their mass, have been used as powerful devices for cluster research.

Alkali metal and coinage metal (Cu, Ag and Au) have a valence electron for each atom. For example, silver atom has an electronic structure of [Kr] $[4d]^{10}$ $[5s]$. The stabilities of their clusters are interpreted by a electronic shell model, in which independent delocalized valence electrons are bound in a spherically symmetric potential well. Odd-even alternations and shell effects for these clusters are observed in their mass spectra [7, 8]. When the number of total valence electrons is shell-closed or even number, the cluster is rather stable. In the case of silver

cluster cation, Ag_n^+, the magic numbers are 3, 9, 19, 21, etc. Silver clusters are particular interest due to their role in photographic processes [9] and the stabilities analogous to atomic nucleus. Thus many investigations on physical and chemical properties, such as ionization potentials [10], and fragmentation pathways [11], of silver clusters have been performed. The size-specific reactivities of silver cluster with small molecules such as alcohols [12], C_2H_4, C_6H_6 and NH_3 [13] are also studied. However, the reactions of silver clusters with crown ethers have not been studied.

The purpose of this thesis is to investigate the ion/molecule reactions of silver cluster cations with crown ether. For observing the reactions, a cylindrical ion trap time-of-flight (TOF) mass spectrometer was constructed. Some preliminary tests and the observations of the reactions of alkali metal cations with crown ether were performed for checking the performance of the apparatus. The ion/molecule reactions of Ag_n^+ (n = 1, 3, 5, 7 and 9) were observed and the reaction pathways were determined.

The outline of this thesis is as follows:

Chapter 2:

A cylindrical ion trap TOF mass spectrometer suitable for observing the ion/molecule reactions was constructed. The technical data for construction and the results of

the tests of the performance are described.

Chapter 3:

Using the apparatus, the ion/molecule reactions of some alkali metal cations with crown ether were observed. The reaction rate constants were obtained. These values were compared to the values reported previously.

Chapter 4:

The ion/molecule reactions of Ag_n^+ (n = 1, 3, 5, 7 and 9) with crown ether were observed and the reaction pathways of each size of cluster were determined. The reaction mechanisms and the informations on the geometrical structures of the silver clusters were also discussed.

References

[1] C. J. Pedersen, J. Am. Chem. Soc. **89**, 2495 (1967).

[2] D. V. Dearden, Y. Liang, J. B. Nicoli, and K. A. Kellersberger, J. Mass Spectrom. **36**, 989 (2001).

[3] P. B. Armentrout, Int. J. Mass Spectrom. **193**, 227 (1999).

[4] N. Shen, R. M. Pope, and D. V. Dearden, Int. J. Mass Spectrom. **195/196**, 639 (2000).

[5] S. E. Hill and D. Feller, Int. J. Mass Spectrom. **201**, 41 (2000).

[6] I. H. Chu, H. Zhang, and D. V. Dearden, J. Am. Chem. Soc. **115**, 5736 (1993).

[7] W. D. Knight, K. Clemenger, W. A. de Heer, W. A. Saunders, M. Y. Chou, and M. L. Cohen, Phys. Rev. Lett. **52**, 2141 (1984).

[8] I. Katakuse, T. Ichihara, Y. Fujita, T. Matsuo, T. Sakurai, and H. Matsuda, Int. J. Mass Spectrom. Ion Proc. **67**, 229 (1985).

[9] P. Fayet, F. Granzer, G. Hegenbart, E. Moisar, B. Pischel, and L. Wöste, Phys. Rev. Lett. **55**, 3002 (1985).

[10] C. Jackschath, I. Rabin, and W. Schulze, Z. Phys. D **22**, 517 (1992).

[11] S. Krückeberg, G. Dietrich, K. Lützenkirchen, L. Schweikhard, C. Walter, and J. Ziegler, Int. J. Mass Spectrom. Ion Proc. **155**, 141 (1996).

[12] P. Sharpe, J. M. Campbell, and C. J. Cassady, Organometallics **13**, 3077 (1994).

[13] M. P. Irion, P. Schnabel, and A. Selinger, Ber. Bunsenges. Phys. Chem. **94**, 1291 (1990).

Chapter 2

Construction of an Ion Trap Time-of-Flight Mass Spectrometer

2.1 Introduction

Quadrupole ion trap, invented by Paul [1], have been widely used for various research fields, including physics, chemistry and biology. Attractive features of the ion trap includes the abilities to store ions at isolation state in vacuum, and to observe processes of reactions directly. Furthermore, a quadrupole ion trap consists of only three electrodes and thus can be constructed easily because of their simplicity. One of the instruments similar to an ion trap, which can store ions for a long time, is Fourier transform ion-cyclotron resonance (FTICR) mass spectrometer. An ion trap does not need a huge and expensive superconducting

magnet such as FTICR device. These features have led to many publications and reviews [2] on gas-phase ion reaction. Recently, various ionization methods such as secondary ion mass spectrometry (SIMS) [3], electrospray ionization (ESI) [4] and matrix-assisted laser desorption/ionization (MALDI) [5] have been combined with ion traps.

Most of the commercially available ion traps are used as mass spectrometers. In these instruments, mass scans are performed by ejection of stored ions according to their mass-to-charge ratio (m/z). In this case, however, the ions are ejected to mainly two directions and only half of these enter the detector. As a consequence, detection sensitivities are limited. Furthermore, to obtain a mass spectrum of high mass range, scanning the relatively high amplitude of radio frequency (rf) voltage is required.

On the other hand, an ion trap can be combined to a time-of-flight (TOF) mass spectrometer. In this case, an ion trap is used only for an ion storage device. All the stored ions are ejected to a TOF mass analyzer. The instruments of this type become attractive because they have merits of ion storage capability of ion trap and high sensitivity of TOF mass spectrometer. The instruments employing an ion trap with a linear TOF mass spectrometer [6] or with ion mirror [7] have been developed. In this study, an ion trap TOF mass spectrometer with four toroidal electric sectors for observing the ion/molecule reactions was constructed. The technical data for construction and the results of tests of the performance are reported.

Principles of quadrupole ion trap

A schematic drawing of a quadrupole ion trap is shown in Fig. 2.1. It consists of a ring electrode and a pair of end-cap electrodes which have hyperbolic inner surfaces. The electric field is generated by applying the rf and dc voltages between the ring electrode and the pair of end-cap electrodes. The potential ϕ at any point (r, z) within the ion trap are given as

$$\phi_0 = U + V\cos\Omega t \tag{2.1}$$

$$\phi(r,z) = \frac{\phi_0}{2r_0}(r^2 - 2z^2) + \frac{\phi_0}{2} \tag{2.2}$$

where U, V, Ω and r_0 are the dc voltage, amplitude of the rf voltage, angular frequency of the rf voltage and the nearest radius of the ring electrode, respectively. In the case of using a cylindrical electrode and a pair of disk electrodes instead of the hyperbolic electrodes, the potential around the center in the ion trap can be approximately expressed by the same equation.

The equations of motion for an ion of mass m and charge e in the ion trap are expressed as

$$\frac{d^2u_i}{d\tau^2} + (a_i - 2q_i\cos 2\tau) = 0 \quad (i = r, z) \tag{2.3}$$

where

$$\tau = \frac{\Omega}{2}t, \tag{2.4}$$

$$a_z = -2a_r = -\frac{8eU}{mr_0{}^2\Omega^2}, \tag{2.5}$$

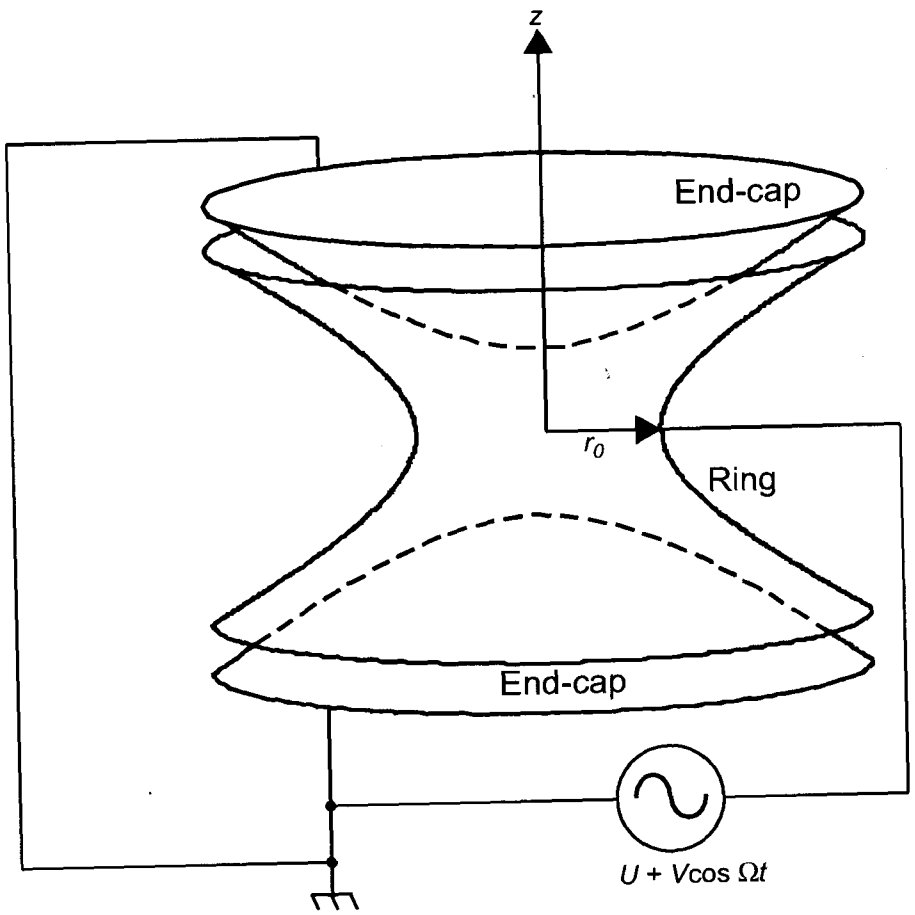

Figure 2.1: Shematic drawing of quadrupole ion trap.

$$q_z = -2q_r = -\frac{4eV}{mr_0{}^2\Omega^2} \tag{2.6}$$

and

$$u_r = r, u_z = z. \tag{2.7}$$

Equation (2.3) is called Mathieu equation, the solutions of which are well known [8]. The complete solution to the Mathieu equation is given as

$$u_i(\tau) = A \sum_{n=-\infty}^{\infty} C_{2n} \cos(2n + \beta_i)\tau + B \sum_{n=-\infty}^{\infty} C_{2n} \sin(2n + \beta_i)\tau. \tag{2.8}$$

The constants A and B depend upon the initial conditions, and C_{2n} and β are the functions of a_i and q_i. Thus, the stability of an ion trajectory depends on the values of a_i and q_i. Such graphical representations of stable solutions to the Mathieu equation are called *stability diagrams*, of which a part is shown in Fig. 2.2. As shown in this figure, only the ions correspond to the points within the stability region are confirmed in the ion trap.

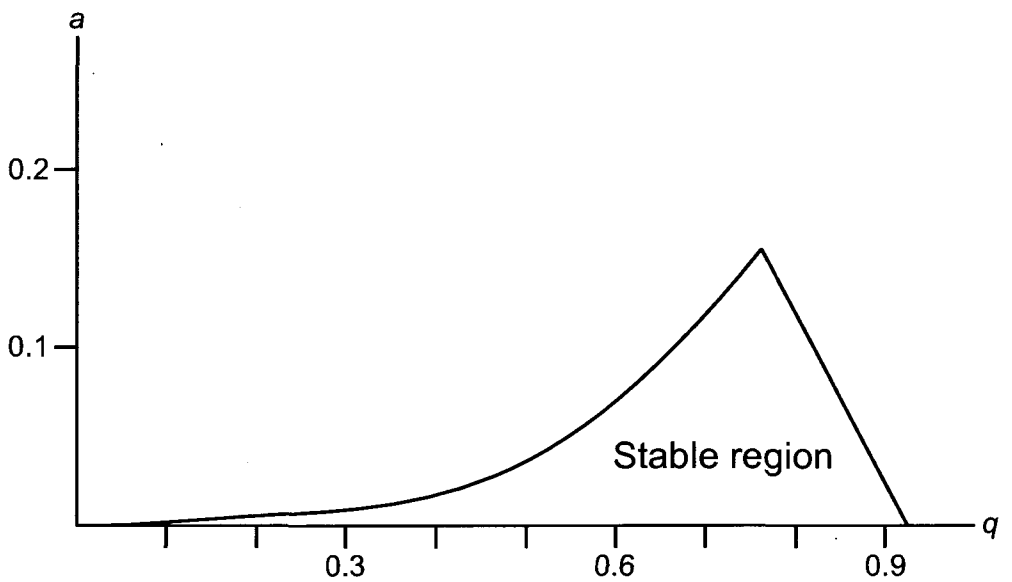

Figure 2.2: Shematic diagram of a part of the stability diagram.

Inside the ion trap, the stored ions are oscillated by the quadrupole field with their eigenfrequencies. The frequency of z-component is given as

$$\omega_z = \beta_z \Omega / 2. \tag{2.9}$$

The approximate relationship [9]

$$\beta_z = (a_z + {q_z}^2/2)^{1/2} \tag{2.10}$$

was validated by direct observation for q <0.4, at which limit the approximation is exceeded by 1%. Therefore, application of a small alternating voltage with their frequency of ω_z causes buildup of motion in the z direction and ejection of the particle from the ion trap (resonance ejection). For instance, when a white noise, which contains all the frequency components, is applied to a end-cap electrode, all the ions stored in the ion trap will be ejected. Applying a certain voltage which corresponds to the eigenfrequency of a specific mass causes a ejection of only ions of the mass. Conversely, applying a voltage which contains all the eigenfrequencies except that of a specific mass will cause a mass-selective storage. Using this method, only the ions of a specific mass can be selected as reactants.

2.2 Construction of a cylindrical ion trap time-of-flight mass spectrometer

2.2.1 Ion source

A schematic diagram of the ion source is shown in Fig.2.3. To produce cluster cations, a sputtering ion source was adopted. The cluster cations were produced by xenon ions bombardment on a sample material. The primary xenon ions are produced by a compact primary gun of a discharge type [10]. A typical discharge current was 0.2 mA. The xenon ions are accelerated up to 12 keV. The secondary ions are accelerated and directed to the ion trap by the electrostatic potential applied to the extraction lens system. This lens system consits of a disk (electrode A in Fig.2.3) and five sets of two-semidisk (electrode B–E in Fig.2.3) electrodes. The outer and inner diameters of the electrode B - E are 70.0 mm and 9.5 mm. The diameters of the lens A are 70.0 mm. The thicknesses of the electrodes are 2.0 mm (electrode A) and 5.0 mm (electrode B -E). The distance between all the electrodes is 5.0 mm. A typical acceleration energy of the secondary ions was 1.30 keV. Typical potentials applied to the lens electrodes were 0.70 kV (electrode A), 0.35 kV (electrode B), 0.83 kV (electrode C), 1.06 kV (electrode D) and 0 V (electrode E). A deflector electrode (ion gate) is mounted at the end of the extraction lens system. The ion gate deflects the ion beam to prevent it from getting into the ion trap during the reaction period. A typical potential applied to the ion gate was 1.10 kV. The ion source was mounted inside the differentially pumped

vacuum chamber.

2.2.2 Deceleration lens system

To extract the secondary ion beam with high efficiency, a high acceleration energy, typically a few keV, is required. However, it is difficult to confine the ions with such a high kinetic energy in the ion trap. The energy range of ions for confinement is required to lie below a few tens eV [2]. Therefore, the deceleration lens system was adopted in order to introduce the ion beam into the ion trap without their divergence. A schematic diagram of the lens system is shown in Fig. 2.4 (electrode F - I). The lens system consists of four cylindrical electrodes. The outer diameter of all the electrodes is 40.0 mm. The inner diameters of the electrodes are 5.0 mm (electrode F) and 10.0 mm (electrode G - I). The thicknesses of the electrodes are 5.0 mm (electrode F, G) and 7.5 mm (electrode H, I). The distance between all the electrodes are 2.5 mm. The potentials applied to these electrodes are adjusted so as to maximize ion intensity. A typical set of these potentials was 0 V (electrode F), 0.80 kV (electrode G), 0 V (electrode H) and 0.85 kV (electrode I). These electrodes were mounted inside the differentially pumped vacuum chamber.

2.2.3 Ion trap

The ions from the deceleration lens system are then injected into the ion trap. A schematic diagram of the ion trap used in this study is shown in Fig. 2.4. The

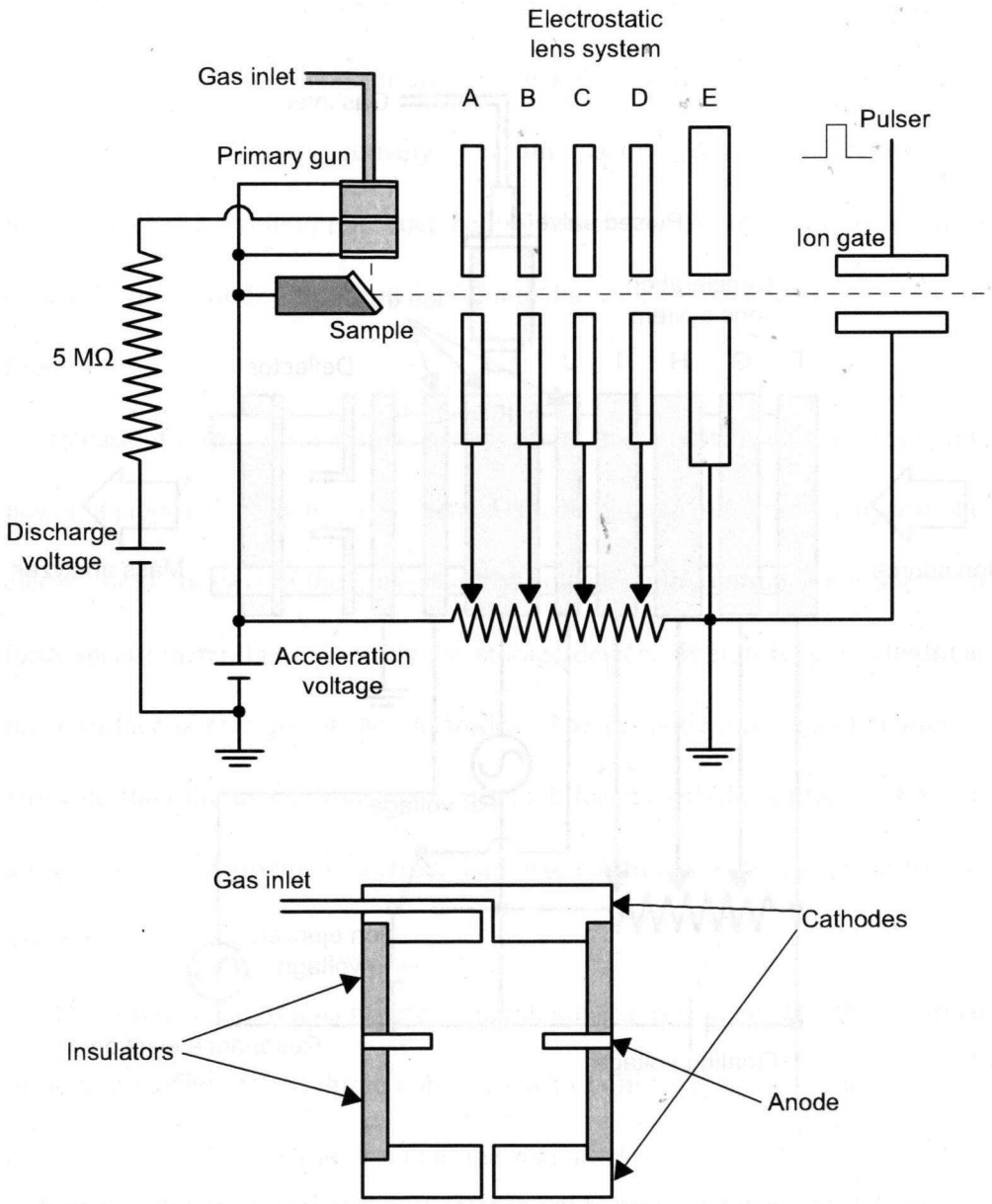

Figure 2.3: Shematic diagram of the ion source.

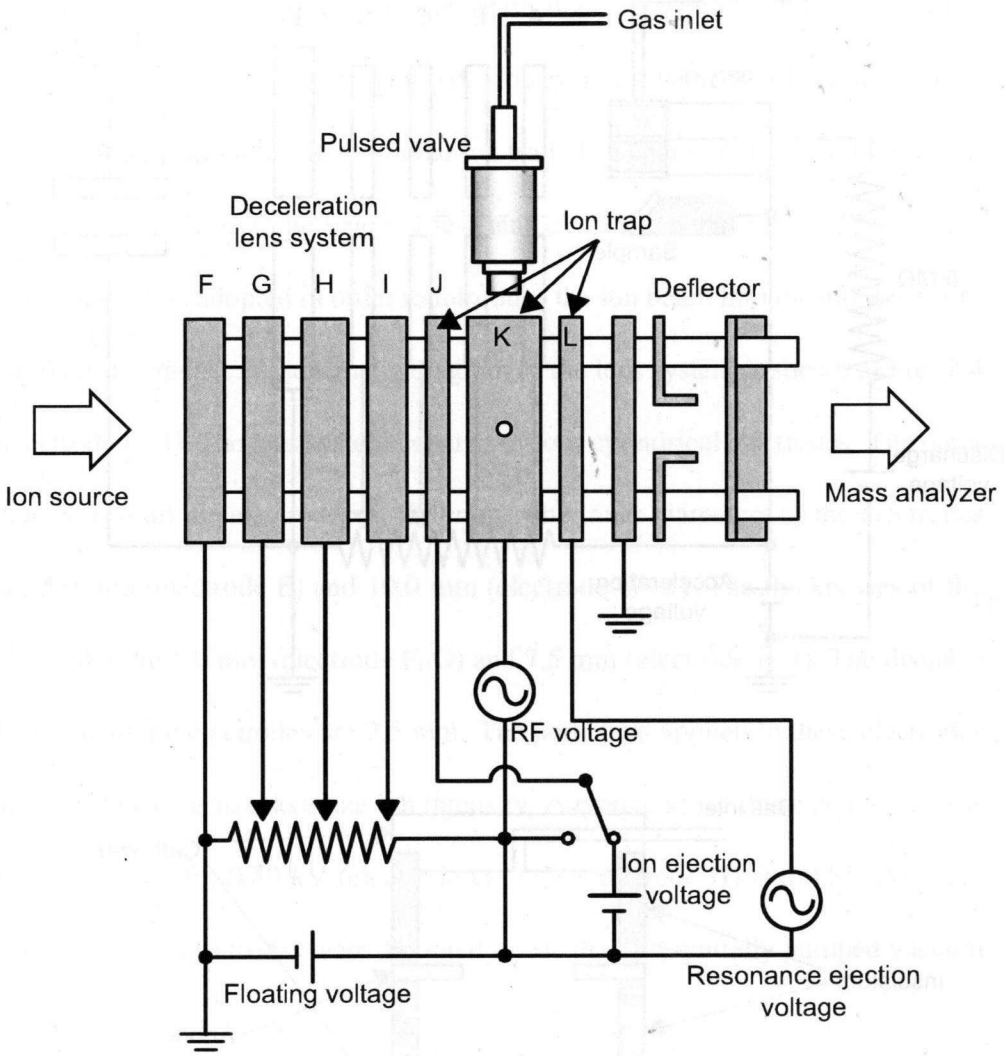

Figure 2.4: Shematic diagram of the deceleration lens system and the ion trap.

ion trap consists of a cylindrical electrode (ring electrode, K in Fig. 2.4) and two disk electrodes (end-cap electrodes, J and L in Fig. 2.4). The inner, outer diameter and the thickness of the ring electrode are 20.0 mm, 40.0 mm and 9.0 mm, respectively. The diameter and the thickness of the end-cap electrodes are 40.0 mm and 3.0 mm, respectively. The ring electrode has four holes of which the diameter is 2.0 mm to introduce helium buffer gas into the ion trap. Each of two end-cap electrodes has a hole of 2.0 mm diameter for injecting or ejecting the ions.

In case of using an ion trap as a mass spectrometer with high mass resolving power, a precise hyperbolic inner surface is required to make a precise hyperbolic electric field. In case of the present study, however, the ion trap is not used as a mass spectrometer, but only as an ion storage device. Therefore, the cylindrical inner surface is enough for the electrodes. The cylindrical ion trap is easier to fabricate than the quadrupole ion trap which has hyperbolic surfaces. For the above reason, a cylindrical electrode and disk electrodes were employed for the ion trap.

The confinement of ions injected into the ion trap is enhanced by the presence of helium buffer gas. Multiple collisions with buffer gas reduce kinetic energy of ions to a level, which is less than the magnitude of the potential well depth, appropriate to the trapping conditions. Pulsed injection of a large quantity gas can achieve effective confinement. Absence of helium atom as third-body molecule, which may participate the reactions during the reaction periods, is also a merit. In order to achieve this, a pulse of helium is introduced through a fuel injector

valve (16450-PD1-023, Honda, Tokyo, Japan) which was modified for helium gas injection. A typical period when the valve opens and peak pressure of helium introduced into the ion trap are 1.5 ms and ca. 5×10^{-3} Pa, respectively. Helium is also used for thermalization of internally hot clusters by a few thousands of collisions [11].

To selectively store the ions of a certain m/z as reactant, a resonance ejection method (see section 2.1) was employed. The voltage for resonance ejection (resonance voltage, frequency range: 1 - 150 kHz with a frequency unit of 1 kHz, amplitude: 0.2 V_{0-p}) for mass-selective storage is applied to the end-cap electrode of front-side (L in Fig. 2.4). The resonance voltage is applied for typically 500 ms after starting ion injection. The numeric data of the resonance voltage is generated by the following procedure: (1) $f_z = \omega_z/2\pi$ (kHz), the eigenfrequency of the ion of a specific mass, is calculated by equation (2.9), (2) all the sine waves except the frequency range of $f_z - \Delta f < f < f_z + \Delta f$ (Δf is several kHz) are summed up as

$$X(t) = 0.2 \left[\sum_{f=1}^{f_z - \Delta f} \sin(2\pi f t + \theta_f) + \sum_{f=f_z+\Delta f}^{150} \sin(2\pi f t + \theta_f) \right] \qquad (2.11)$$

where $X(t)$ and θ_f are the function of the resonance voltage and the initial phase, respectively and (3) the numerical values are obtained by substituting arbitrary t into equation (2.11). Δf is introduced by considering the discrepancy of f_z because of using an approximate quadrupole electric field. The resonance voltage is generated from the numerical data by a digital-to-analog converter (DAC) (NI 6052E, National Instruments, Texas, USA). The sampling rate and the quantiza-

tion bit rate of the DAC is 333 kHz and 16 bit, respectively.

After a storage period, all the ions stored inside the ion trap are ejected to the TOF mass analyzer by a pulsed voltage applied to the end-cap electrode of rear-side (J in Fig. 2.4). The ion trap was mounted inside the differential pumped vacuum chamber together with the deceleration lens system. A schematic diagram of assembly is shown in Fig. 2.4.

2.2.4 Mass analyzer

To determine reaction products with high accuracy, a high mass resolving power is required. A TOF mass spectrometer developed at Osaka University consists of four 269° electric sectors of 50 mm radius [12] was employed in the present study. Each of this sector field consists of cylindrical electrodes with Matsuda plates [13]. This apparatus satisfies triple isochronous focusing (horizontal position, horizontal inclination angle and energy) and triple space focusing (horizontal inclination angle, vertical inclination angle and energy). Mass resolving power 2000 with gramicidin-S ions had been achieved previoulsy [14]. The total flight length of the system is 2.0 m. Typical potentials applied to electrodes were +0.25 kV (outer cylindrical electrode), -0.25 kV (inner cylindrical electrode) and 0.03 kV (Matsuda plate). A schematic diagram and a photograph of the total system is shown in Fig. 2.5 and 2.6, respectively.

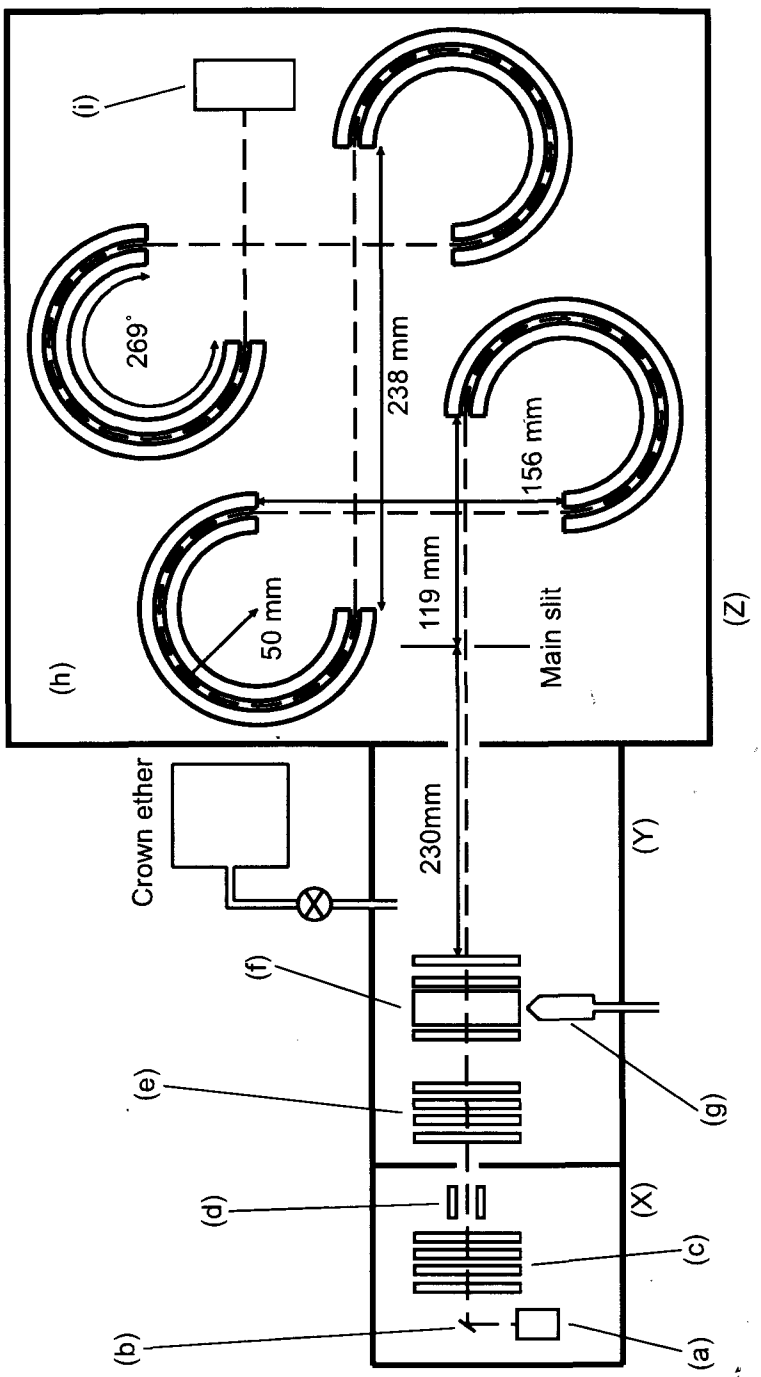

Figure 2.5: Shematic diagram of the apparatus. (a) Primary gun, (b) sample target, (c) extraction lens system, (d) ion gate, (e) deceleration lens system, (f) ion trap, (g) pulsed valve, (h) TOF mass analyzer and (i) MCP detector. (X), (Y) and (Z) vacuum chambers.

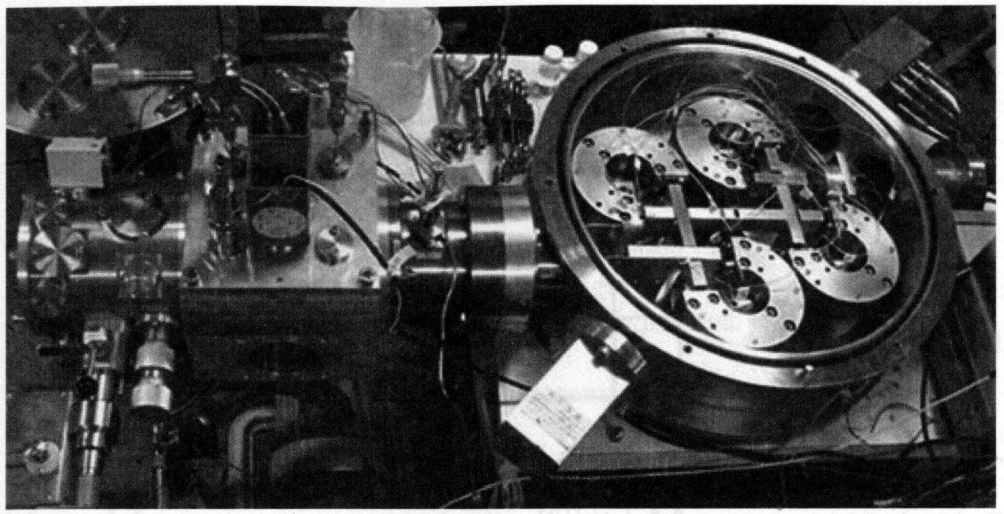

Figure 2.6: Photograph of the apparatus.

2.2.5 Operating system and electric circuits

A timing chart of a measurement is shown in Fig. 2.7. The digital output board (PCI-2472C, Interface, Hiroshima, Japan) provides all the timing signals. The digital output board is controled by the program using LabView 6.1 (National Instruments).

RF amplifier and switching circuit

The rf driving voltage is applied to the ring electrode by the hand-made rf amplifier and resonance circuit [15] (Fig.2.8). The typical amplitude of the rf signal from a mutifunction synthesizer (1940, NF electronic instruments, Yokohama, Japan) is 2.5 V_{p-p}. Then the rf signal is amplified by the operational amplifier, source-followers and the transformers. The total amplification rate of the circuit is about 200. The maximam potential and the frequency range of this circuits

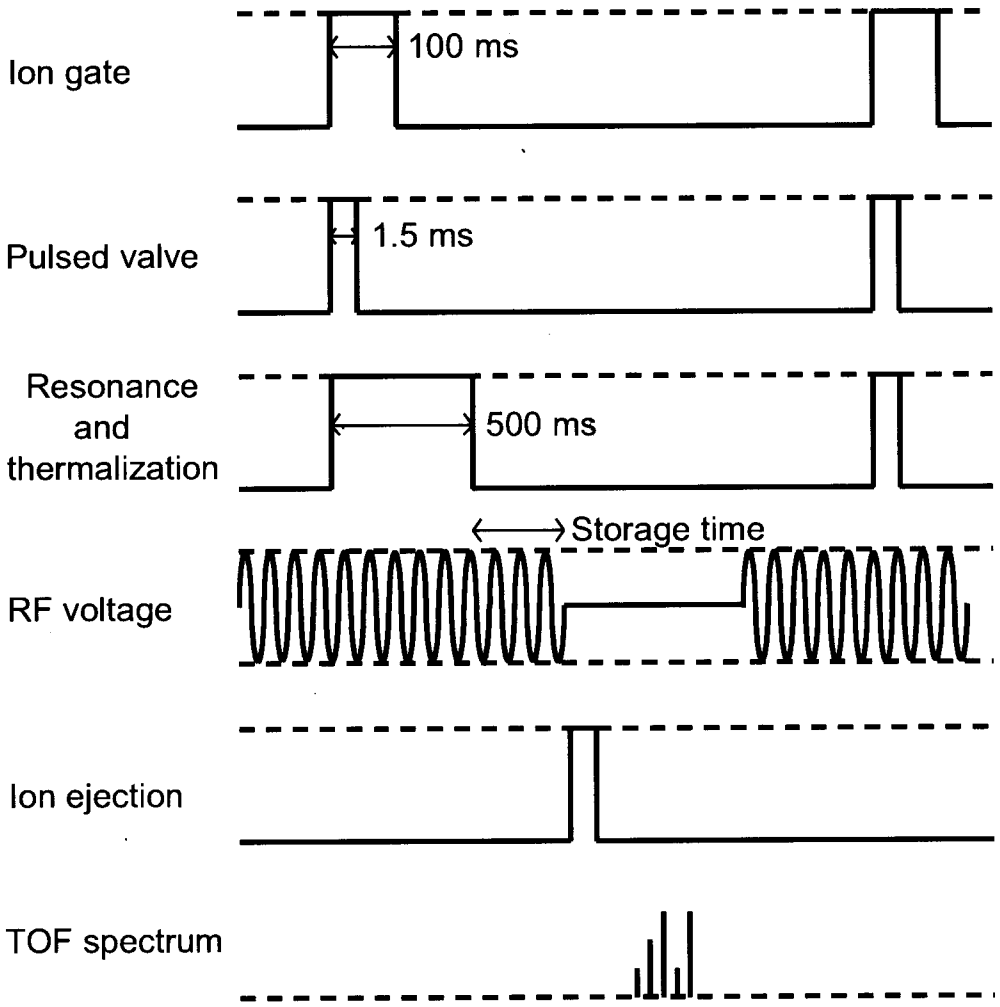

Figure 2.7: Timing chart of a measurement.

are 0.65 kV_{0-p} and 500 kHz - 1.2 MHz, respectively. If the rf driving voltage is applied during ion ejection, the ion acceleration energy alters by the rf voltage which is superimposed on the pulsed voltege for ion ejection [16]. Consequently, the mass resolving power of the apparatus is decreased. To avoid this effect, the circuit which can turn off the rf voltage rapidly (within ca. 1 μs) synchronized with TTL signals for ejection of ions was constructed. The rapid turning off, i.e. short-circuit, is achieved by MOS FETs. Because of electric isolation between input TTL and the rf output, the rf voltage can be easily electrically floated. The circuit diagram of the switch is shown in Fig. 2.9.

Two-stage acceleration and high voltage switching circuit

In order to compensate for the flight time deviation caused by the initial position of ions in the ion trap, a two-stage acceleration method proposed by Wiley and McLaren [17] was employed. This is effective method to focus the ions distributing inside the ion trap on the detector. The focusing condition is given as

$$L = 2S_0{k_0}^{3/2}\left(1 - \frac{D}{(k_0 + {k_0}^{1/2})S_0}\right), \tag{2.12}$$

$$k_0 = \frac{S_0E_s + DE_d}{S_0E_s} \tag{2.13}$$

where L, S_0, D, E_s and E_d are the focal length, the length of the first acceleration field, the length of the second acceleration field, the electric field strength of the first acceleration field and the electric field strength of the second acceleration field, respectively. The TOF mass spectrometer is designed so as that a focusing

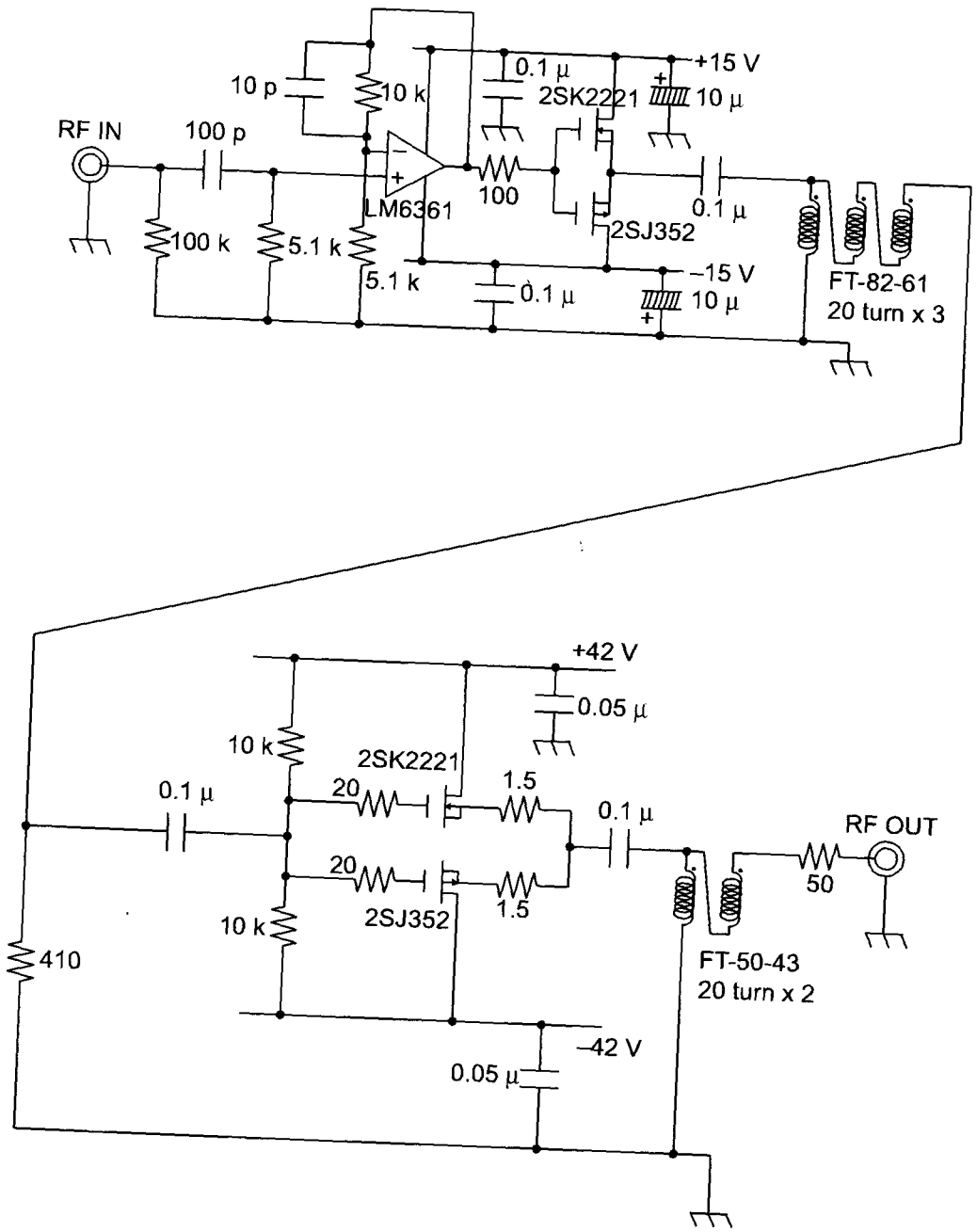

Figure 2.8: Circuit diagram of the rf amplifier.

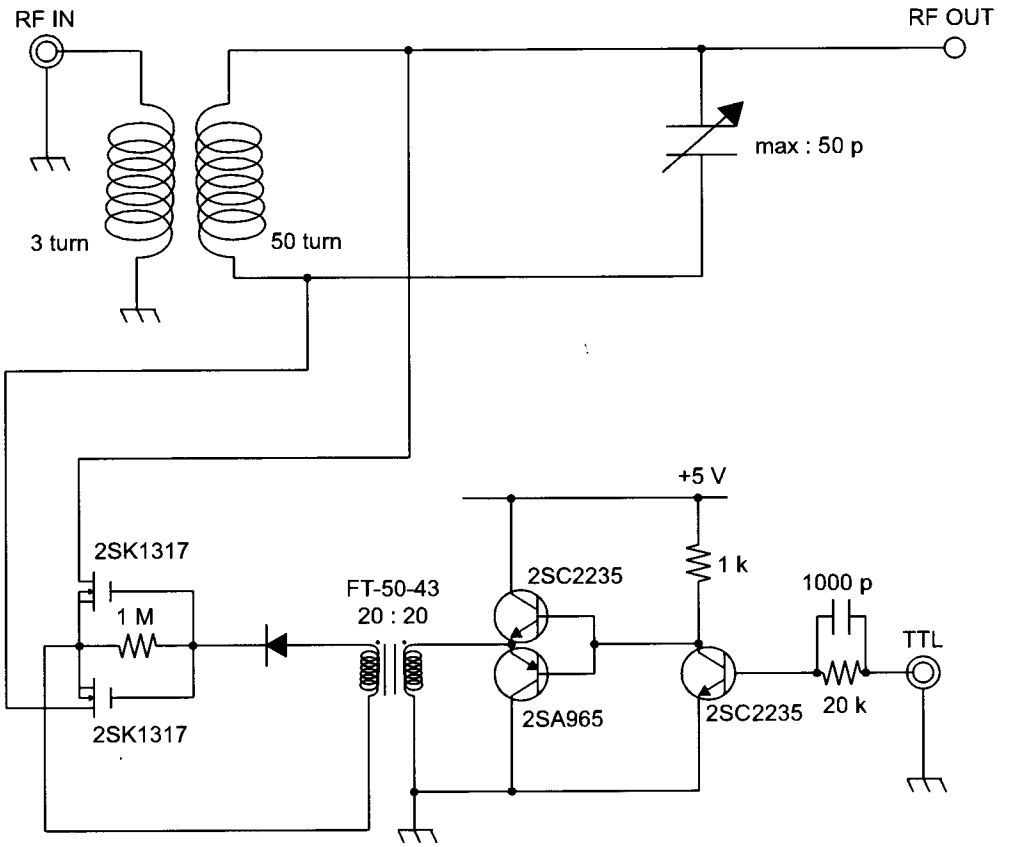

Figure 2.9: Circuit diagram of the rf resonance and switching circuit.

at the detector is achieved by focusing the ions at the position of the main slit [12]. Therefore, the focal length, L, can be regarded as the length from the acceleration region to the main slit. In the conditions of the apparatus, $L = 230$ mm, $S_0 = 7$ mm, $D = 7$ mm, $E_s = V_a/L_2$ and $E_d = V_{float}/L_1$ where V_{float}, V_a, L_1 and L_2 represent the second and the first acceleration voltages, the length of the second and the first acceleration region ($L_2 = 14$ mm and $L_1 = 7$ mm), respectively. Thus the appropriate voltage ratio applied to the electrodes of the first and second acceleration grids can be calculated as

$$V_{float} \approx 3V_a. \tag{2.14}$$

A pulsed voltage of a few kV for ion acceleration is required for the mass analyzer used in the present study. Thus, a high voltage switching circuit have been constructed (Fig. 2.10). This circuit is a push-pull switch employing MOS FETs. A rise time of the pulsed voltage is within 100 ns. The input signals do not have to be electrically floated because electric isolation between input and output is achieved by optocouplers.

2.2.6 Detector and data acquisition system

A two-stage micro-channel plate (MCP) detector (F4655-10, Hamamatsu Photonics, Shizuoka, Japan) was used in this study. A typical potential applied to this MCP was -2.1 kV. The typical gain of the detector is about 10^6. The signals from the detector are averaged (20–100 measurements for each reaction time) on a digital oscilloscope (LC564AD, LeCroy Japan, Osaka, Japan).

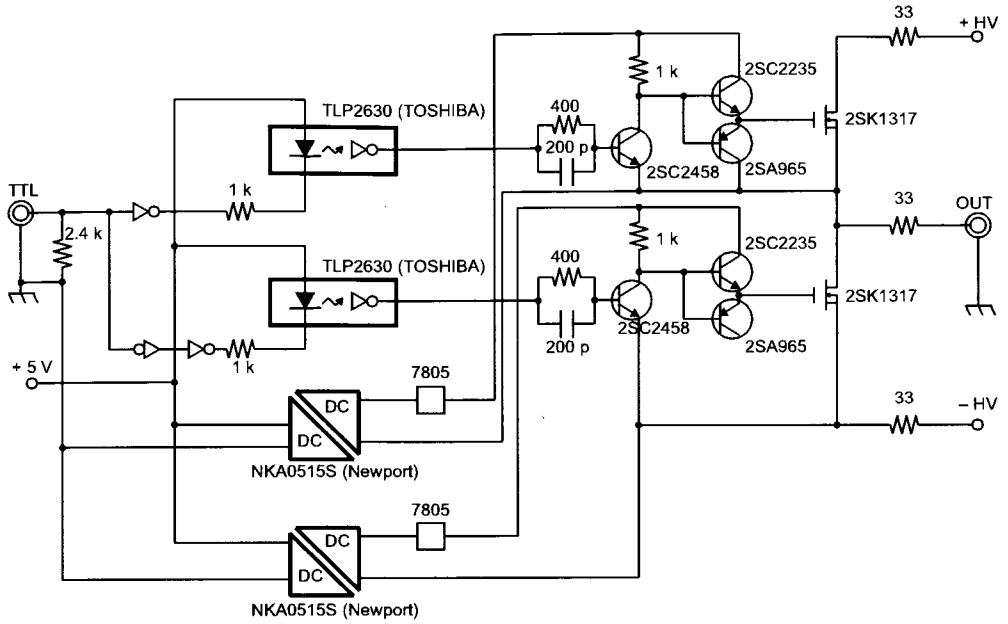

Figure 2.10: Circuit diagram of the high voltage switching circuit.

2.3 Performance of the ion trap time-of-flight mass spectrometer

For testing the constructed apparatus, some experiments were performed. These experiments include testing the mass resolving power, the quantitativity of the ion intensity and the selectivity of the resonance ejection.

The common operating conditions of the measurements were (1) the acceleration energy of the primary xenon ions was 12 keV, (2) the acceleration energy of the secondary cluster cations was 1.11 keV, (3) the first-stage acceleration voltage (V_a) for ejecting ions to the mass analyzer was 0.93 kV and (4) the second-stage acceleration voltage (V_{float}) for ejected ions was 1.10 kV.

Mass resolving power

The TOF spectra of Ag_n^+ (n = 1–3) are shown in Fig. 2.11. These spectra were obtained under the condition that the rf frequency was 950 kHz, the rf voltage was 500 V_{0-p} and the storage time was 0 s. The storage time is defined as the time interval from the end of applying the resonance voltage to the moment applying the pulsed voltage for ion ejection. The ordinate is normalized so that the peak hight of $^{107}Ag^+$ is 100. As shown in the Fig.2.11 (b) and (c), each peak of the cluster is separated according to their isotopic compositions. The mass resolving power calculated with the full width at half-maximum (FWHM) of $^{107}Ag^+$ is 370. The ratio of the acceleration voltages (V_a and V_{float}) of this experiments do not satisfy the appropriate voltage conditions calculated from the equation (2.14). For obtaining higher signal intensities of relatively small amount of ions such as cluster, however, higher pulsed acceleration voltage (V_a) was preferred. To achieve higher mass resolving power, higher V_{float} is required as the pulsed acceleration voltage becomes higher. In the present conditions, however, V_{float} more than the present value is difficult to be applied owing to the problem of the circuits. Therefore, the acceleration voltages were selected for the present values in the observations of cluster cations.

Selectivity of the resonance ejection

As described above, the resonance ejection has been employed for selecting the ions with specific m/z as reactants. For testing this functions, the experiments for examining whether only the cluster ions with specific size can be stored were

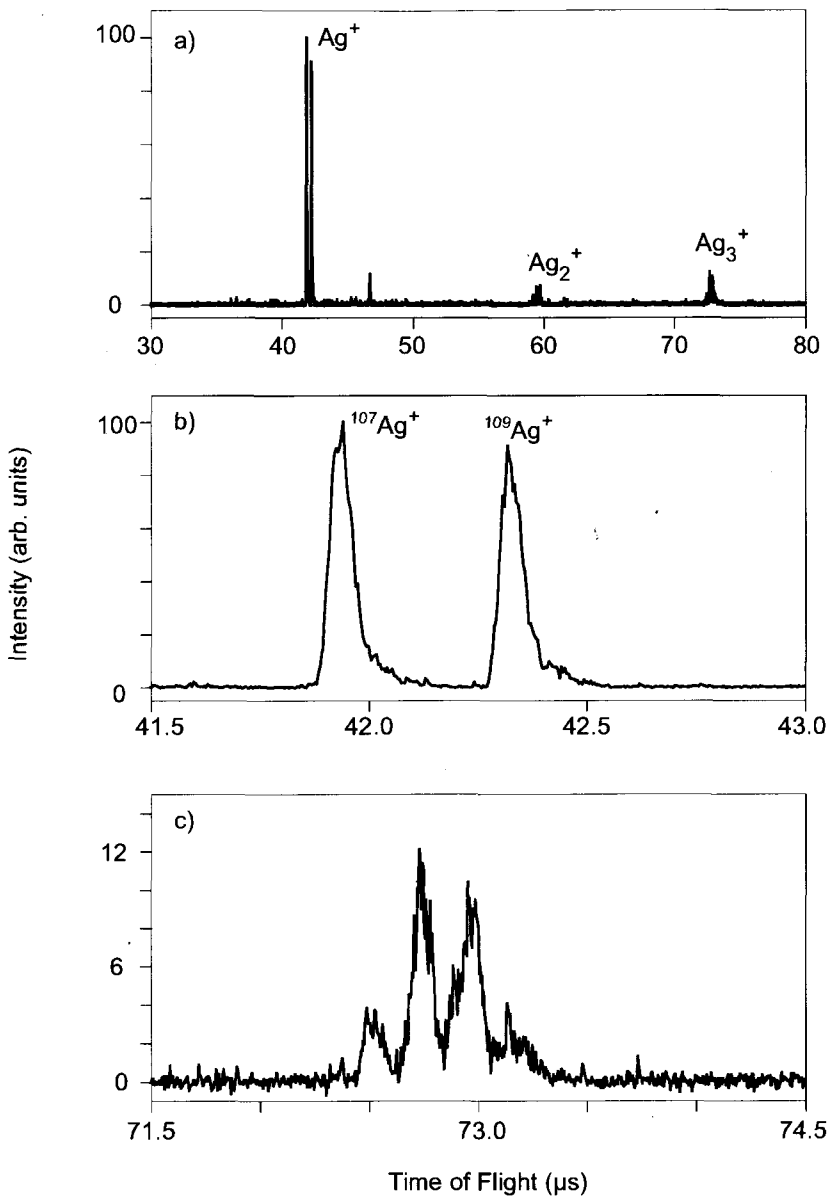

Figure 2.11: TOF spectra of Ag_n^+ (n = 1–3). (a) whole TOF spectrum, (b) expansion of Ag^+ and (c) expansion of Ag_3^+.

performed.

The operating conditions for selecting only Ag^+ were (1) the rf frequency was 950 kHz, (2) the rf voltage was 500 V_{0-p}, (3) the frequencies of the resonance voltage were 1–95 and 111–150 kHz (calculated resonance frequency: 168 kHz), (4) the ion injection time was 100 ms and (5) the storage time was 0 s. The operating conditions for selecting Ag_n^+ (n = 3, 5, 7 and 9) were (1) the rf frequency was 600 kHz, (2) the rf voltage was 600 V_{0-p}, (3) the frequencies of the resonance voltage were 1–110 and 126–150 kHz, 1–59 and 76–150 kHz, 1–49 and 58–150 kHz, 1–36 and 41–150 kHz for storing Ag_3^+, Ag_5^+, Ag_7^+ and Ag_9^+, respectively, (calculated resonance frequency: 107 kHz for Ag_3^+, 64 kHz for Ag_5^+, 46 kHz for Ag_7^+ and 36 kHz for Ag_9^+), (4) the ion injection time was 100 ms and (5) the storage time was 0 s.

The TOF spectra of Ag^+ obtained using the resonance ejection techniques are shown in Fig.2.12. The ordinate is normalized so that the peak hight of $^{107}Ag^+$ in Fig.2.12 (a) is 100. It is clear that only the Ag^+ is stored using the resonance ejection.

The TOF spectra of Ag_n^+ (n =3, 5, 7 and 9) obtained using the resonance ejection techniques is shown in Fig.2.13. The ordinate is normalized so that the peak hight of Ag_3^+ in Fig.2.13 (a) is 100. It is also clear that only the cluster cations with specific size are stored under the resonance ejection conditions. From these results, it was confirmed that the resonance ejection techniques are valid for selecting the specific cations as a reactant.

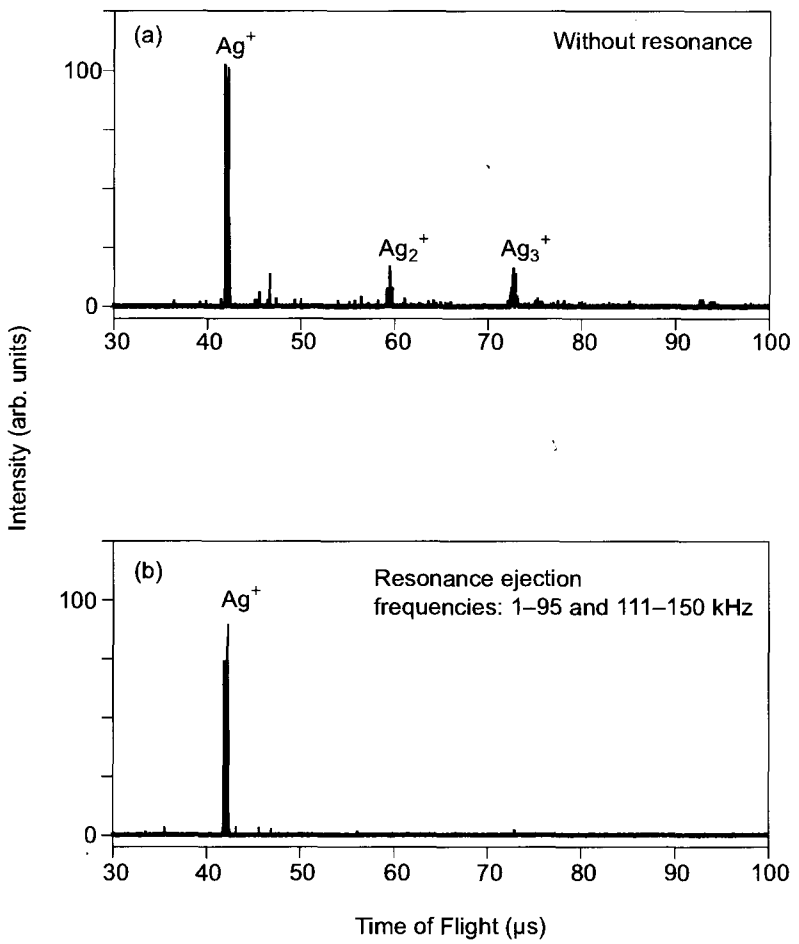

Figure 2.12: TOF spectra of $Ag_n{}^+(n = 1–3)$. (a) whole TOF spectrum obtained without using the resonance ejection, (b) spectrum obtained with using the resonance ejection of frequencies of 1–95 and 111–150 kHz.

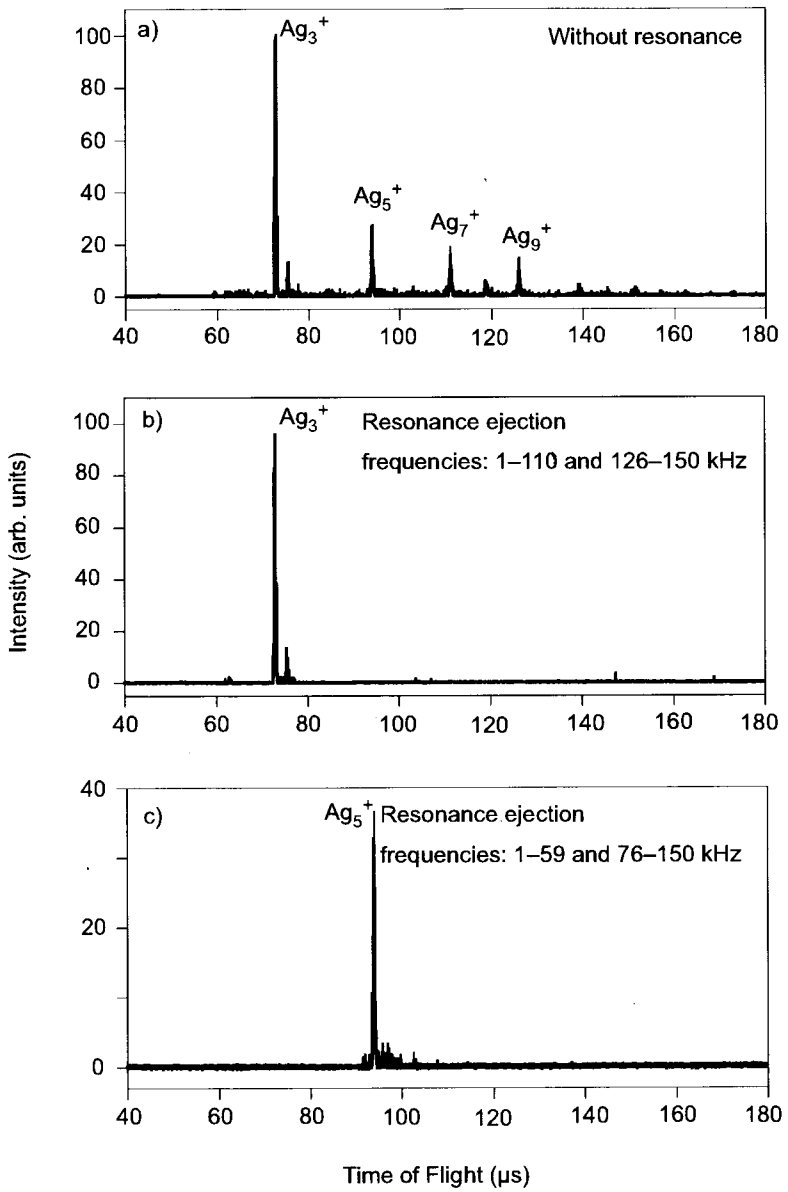
a)
Ag_3^+
Without resonance
Ag_5^+
Ag_7^+
Ag_9^+
b)
Ag_3^+
Resonance ejection
frequencies: 1–110 and 126–150 kHz
c)
Ag_5^+
Resonance ejection
frequencies: 1–59 and 76–150 kHz
Intensity (arb. units)
Time of Flight (μs)

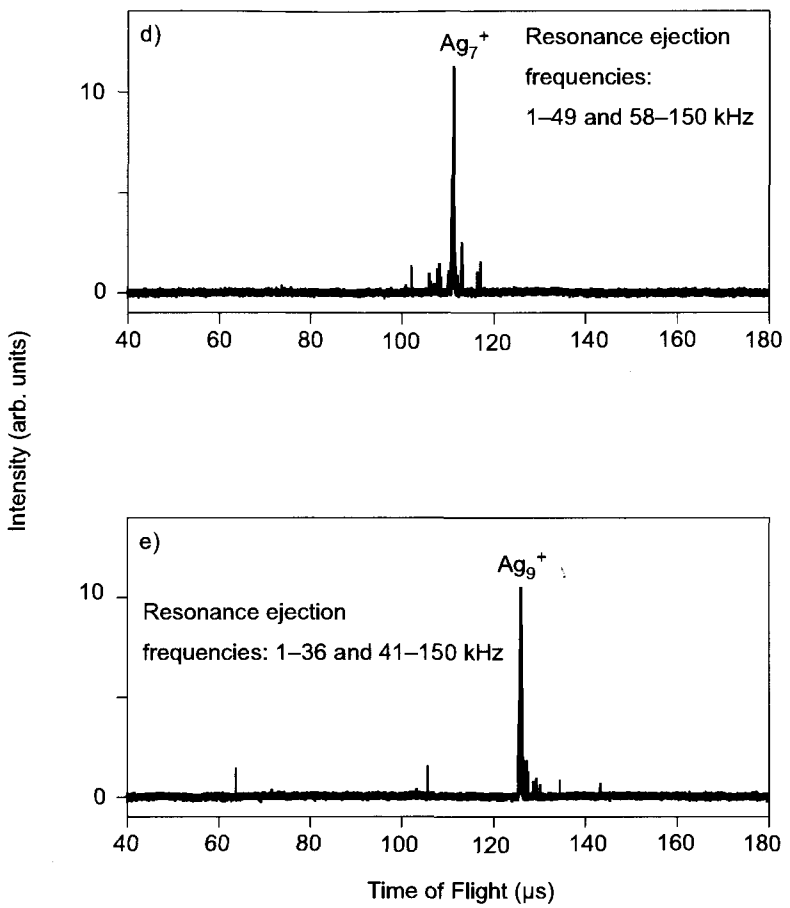

Figure 2.13: TOF spectra of Ag_n^+ (n = 3, 5, 7 and 9). (a) whole TOF spectrum without using the resonance ejection, (b) spectrum with using the resonance ejection of the frequencies of 1–110 and 126–150 kHz, (c) frequencies of 1–59 and 76–150 kHz, (d) frequencies of 1–49 and 58–150 kHz and (e) frequencies of 1–36 and 41–150 kHz.

Quantitativity of ion intensities

For determining the reaction pathways or rate constant of the ion/molecule reactions, the quantitativity of the ion intensities are also important factor. In the present study, the ion trap was operated in the conditions of $a_z = a_r = 0$ in the equation (2.5). Thus, in principle, all the ions with higher m/z than the lower limit determined by $q_z = 0.908$ can be stored. In practice, however, by the space charge effect or potential difference from the precise quadrupole field resulting from using the cylindrical electrodes, the *storage lifetime*, i.e. the mean period when the ions can be stored, may differ by q_z. For checking the *storage lifetimes* for various q_z, the *lifetimes* of Ag^+ were measured under the various q_z calculated by the equation (2.6). The experimental conditions were follows: the rf frequencies and voltages were (1) 790 kHz with 500 V_{0-p} ($q_z = 0.72$), (2) 800 kHz with 450 V_{0-p} ($q_z = 0.64$), (3) 950 kHz with 500 V_{0-p} ($q_z = 0.50$), (4) 950 kHz with 420 V_{0-p} ($q_z = 0.42$), (5) 920 kHz with 350 V_{0-p} ($q_z = 0.37$), (6) 1020 kHz with 250 V_{0-p} ($q_z = 0.22$) and (7) 1100 kHz with 250 V_{0-p} ($q_z = 0.19$); the storage times were 0 s, 1.5 s, 3.0 s and 5.0 s for each rf condition.

The TOF spectra of Ag^+ obtained under the condition that the rf frequency and voltage were 920 kHz and 350 V_{0-p}, respectively with using the resonance ejection of the frequencies of 1–114 kHz are shown in Fig.2.14. The ordinate is normalized so that the peak hight of Ag^+ at the storage time of 0 s is 100. Fig.2.14 (c) shows the storage time dependence of the ion intensity. It is seen that the ion intensity displays an approximately exponential fall-off. Thus the data points were

subjected to least-squares fitting of

$$I(t) = 100 \exp(-t/T) \tag{2.15}$$

where t, $I(t)$ and T are the storage time, ion intensity and the *lifetime*. The fitted curve is shown in Fig.2.14 (c).

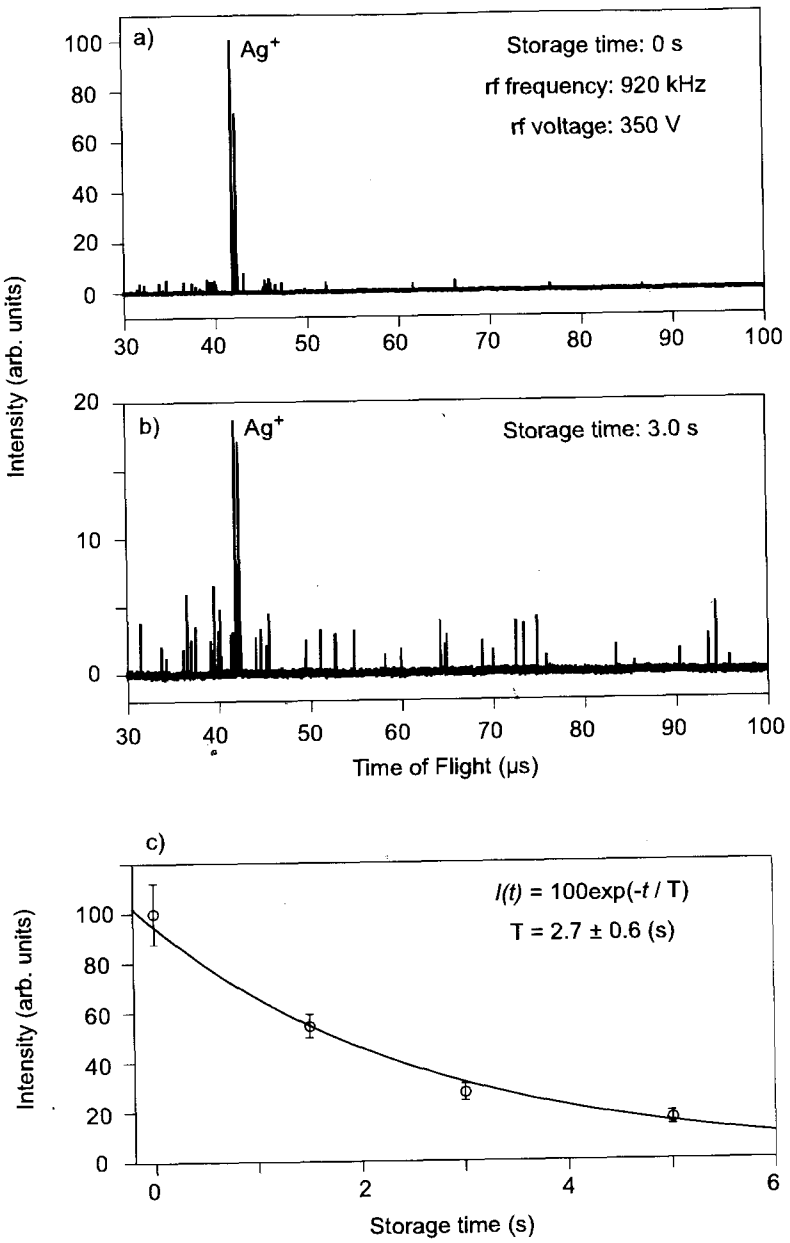

Figure 2.14: TOF spectra and storage time dependence plot of the intensity of Ag^+. The frequencies applied for the resonance ejection were 1–114 kHz. (a) and (b) TOF spectrum at the storage time of 0 s and 3.0 s, respectively and (c) Storage time dependence of the intensity. The curve in (c) is least-squares fitting curve. The error bars represent standard deviations of four measurements.

The variations of the *lifetime*, T, with the calculated value of q_z is shown in Fig.2.15. The open circles in the figure represent the data obtained under the resonance ejection condition. The filled circles represent the data obtained without resonance ejection. Under the conditions of $q_z > 0.72$, Ag^+ was not observed. Therefore, the practical upper limit of the q_z was found to 0.72.

In the both cases, the variations of the *lifetime* are not so simple. The scattering of the lifetimes with q_z are considerably large. A correlation between the *lifetimes* and q_z was not confirmed. Thus the *lifetimes* can be regarded as constant within the experimental error. However, the difference between minimum and maximum values of *lifetimes* is ca. 2 s. Consequently, in the case of drawing quantitative informations with this apparatus, it is necessary to take into consideration of these scattering.

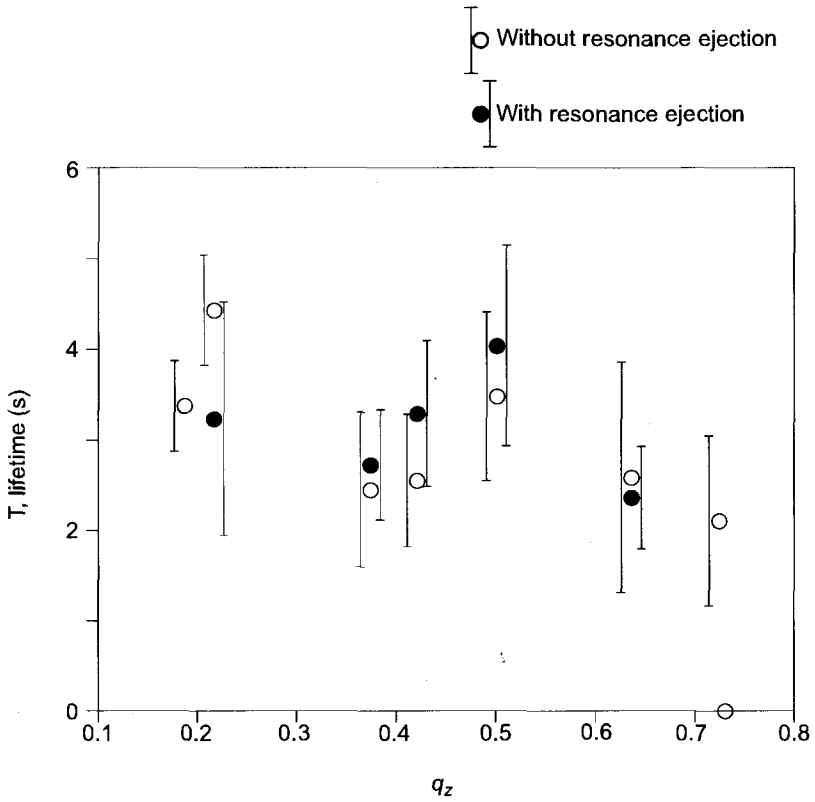

Figure 2.15: Variations of the *lifetime*, T, of Ag^+ with calculated q_z. The open circles and the filled circles are the data obtained with resonance ejection and without resonance ejection, respectively. The error bars show the standard errors calculated by least-squares fitting. The error bars positioned on the left side of the open circles are errors of lifetime with resonance ejection. The error bars on the right side of the filled circles are errors without resonance ejection.

2.4 Conclusion

The cylindrical ion trap time-of-flight mass spectrometer has been constructed and their performance has been investigated. It has been confirmed that the silver cluster cations, Ag_n^+ (n = 1–9), have been generated and confined in the ion trap. Using the resonance ejection techniques, selectively storage of the specific size of cluster has been achieved. Although the quantitative performance of the cylindrical ion trap is not good for storage the ions, considering the crudity, simplicity and easy-fabricate of the device are merits for investigating the ion/molecule reactions. This apparatus can be used for many investigations on ion/molecule reactions of various metal cluster cations in the future.

References

[1] W. Paul and H. Steinwedel, Z. Naturforsch. **8a**, 448 (1953).

[2] R. E. March and R. J. Huges, *Quadrupole Storage Mass Spectrometry*, Wiley, New York, 1989.

[3] R. E. Kaiser, J. N. Louris, L. W. Amy, and R. G. Cooks, Rapid Commun. Mass Spectrom. **3**, 225 (1989).

[4] G. J. V. Berkel, G. L. Glish, and S. A. McLuckey, Anal. Chem. **62**, 1284 (1990).

[5] V. M. Doroshenko and R. J. Cotter, Rapid Commun. Mass Spectrom. **7**, 822 (1993).

[6] R. W. Purves and L. Li, J. Am. Soc. Mass Spectrom. **8**, 1085 (1997).

[7] V. M. Doroshenko and R. J. Cotter, J. Mass Spectrom. **33**, 305 (1998).

[8] N. W. McLachlan, *Theory and Applications of Mathieu Functions*, Clarendon, Oxford, 1947.

[9] R. F. Wuerker, H. Shelton, and R. V. Langmuir, J. Appl. Phys. **30**, 342 (1959).

[10] I. Katakuse, T. Ichihara, H. Nakabushi, T. Matsuo, and H. Matsuda, Mass Spectrosc. **31**, 111 (1983).

[11] O. Ingólfsson, H. Takeo, and S. Nonose, J. Chem. Phys. **110**, 4382 (1999).

[12] T. Sakurai, Y. Fujita, T. Matsuo, H. Matsuda, I. Katakuse, and K. Miseki, Int. J. Mass Spectrom. Ion Proc. **66**, 283 (1985).

[13] H. Matsuda and Y. Fujita, Int. J. Mass Spectrom. Ion Phys. **16**, 395 (1975).

[14] T. Sakurai, *The Investigation of a New Time-of-Flight Mass Spectrometer*, PhD thesis, Osaka University, 1987.

[15] K. Kumondai, M. Toyoda, K. Iwamoto, D. Okumura, M. Ishihara, M. Kimura, and I. Katakuse, J. Mass Spectrom. Soc. Jpn. **50**, 217 (2002).

[16] S. M. Michael, M. Chien, and D. M. Lubman, Rev. Sci. Instrum. **26**, 1150 (1992).

[17] W. C. Wiley and I. H. McLaren, Rev. Sci. Instrum. **26**, 1150 (1955).

Chapter 3

Observation of Ion/Molecule Reactions of Alkali Metal Cations with Crown Ether

3.1 Introduction

As described in chapter 1, many experimental [1, 2] and theoretical [3] investigations on gas-phase reactions of metal cations with crown ether have been performed. These investigations are very important from the standpoint of understanding molecular recognition, which is based on size- or shape-specific interactions between molecules. Armentrout [4] reported the trends in the bond dissociation energies for the binding of the alkali metal cations with crown ethers using a collision-induced dissociation (CID) mothod. These theoretical values were also reported [5]. According to these reports, the bond dissociation energies

increase as the cation size becomes smaller. The reaction rate constants of alkali metal cations with crown ethers have been reported [6]. It has been reported that the efficiencies of 1:1 complexations increase with the charge density, i.e. the reciprocal of their volume, of the alkali metal cations. It has also been reported that the optimum reaction efficiency occurs at a cation:cavity ratio of about 1.25:1.

In these works, mainly FTICR mass spectrometers have been used for observing the reactions. The merits of the FTICR devices are high mass resolving power and ion storage capability for a long time. In principle, however, the FTICR requires superconducting magnets and ultra high vacuum conditions. On the other hand, the quadrupole ion traps have the merits of their versatility and ease-of-use. Specially, a cylindrical ion trap is much easier to be fabricated. However, few investigations on the ion/molecule reactions are performed with the cylindrical ion trap because of the problem of their quantitativity. Thus the examinations that the apparatus is work with similar performance of other type of apparatus is required. In this chapter, the observations of the ion/molecule reactions of some alkali metal cations with crown ether are reported. The reaction rate constants are obtained and discussed by comparing to the previous report.

3.2 Experimental

For examining that the constructed apparatus works as a device for observing ion/molecule reactions, the reactions of some alkali metal cations (K^+, Rb^+ and Cs^+) with 15-crown-5 (15C5) were observed. Crown ether, 15C5 (035-16901,

Wako Pure Chemical Industries, Osaka, Japan), was introduced continuously into the vacuum chamber (chamber Y in Fig.2.5) through a leak valve. The pressure of the 15C5 was controlled so as to be kept constant during the measurements by monitoring a ionization gauge (M-430HG, ANELVA, Tokyo, Japan).

To generate alkali metal cations, a surface ionization (SI) method was employed. In SI method, neutral atoms of ionization potential I are heated on a hot metallic surface of work function W and temperature T. The efficiency of ionization is given by the Langmuir-Saha equation,

$$n^+/n_0 = \exp[e(W - I)/kT] \tag{3.1}$$

where n^+, n_0, k and e are the number of cations, the number of total evaporated particles, the Boltzmann's constant and the electric charge, respectively. As seen in the equation (3.1), high ionization efficiency is achieved when the ionization potential of the sample is low and the work function of the metal is high. Thus, this method is effective for ionization of alkali metal, which has relatively low I. In the present study, mixtures of M_2CO_3 (M are K, Rb and Cs), Al_2O_3 and $2SiO_2$ were melted on the platinum foil welded to the tungsten filament. The cations generated by this source were injected into the ion trap through the hole of the ring electrode. The schematic diagram of the ion trap with the ion source is shown in Fig.3.1.

In these experiments, the resonance ejection for selecting the specific ions as the reactant was not employed because the no other cations without reactant alkali metal was generated. Reaction products were stored in the ion trap during the ion

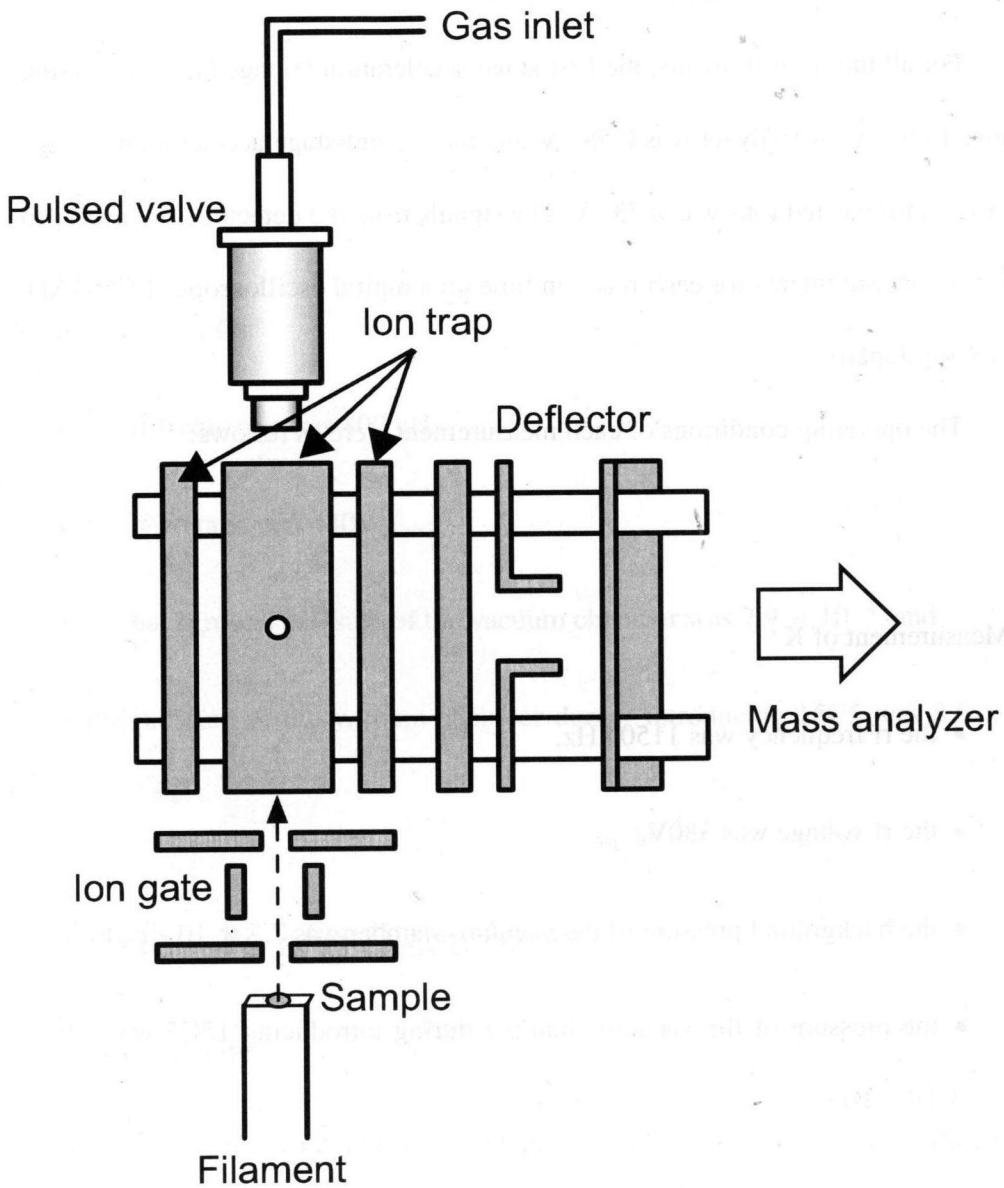

Figure 3.1: Shematic diagram of the ion trap with the SI ion source.

injection period. Thus the storage time, i.e. the reaction time, is defined as the time interval from the starting of the ion injection to ejection of stored ions. The reaction times were varied from 0.05 to 5.05 s.

For all the measurements, the first-stage acceleration voltage (V_a) for ejecting ions to the mass analyzer was 0.58 kV and the second-stage acceleration voltage (V_{float}) for ejected ions was 0.73 kV. The signals from the detector were averaged for 50 measurements for each reaction time on a digital oscilloscope (LC564AD, LeCroy Japan).

The operating conditions of each measurement were as follows:

Measurement of K^+

- the rf frequency was 1150 kHz,
- the rf voltage was $380V_{0-p}$,
- the background pressure of the vacuum chamber was 7.7×10^{-4}, and
- the pressure of the vacuum chamber during introducing 15C5 was 7.9×10^{-4} Pa.

Measurement of Rb^+

- the rf frequency was 1070 kHz,

- the rf voltage was $450V_{0-p}$,
- the background pressure of the vacuum chamber was 8.2×10^{-4}, and
- the pressure of the vacuum chamber during introducing 15C5 was 8.7×10^{-4} Pa.

Measurement of Cs^+

- the rf frequency was 800 kHz,
- the rf voltage was $440V_{0-p}$,
- the background pressure of the vacuum chamber was 7.9×10^{-4}, and
- the pressure of the vacuum chamber during introducing 15C5 was 8.6×10^{-4} Pa.

3.3 Results and Discussion

Observed species

The TOF spectra of the reaction products with some reaction times are shown Fig.3.2–3.4. The ordinates of each figure are normalized so that the peak hight of K^+, Rb^+ and Cs^+ at the reaction time of 0.05 s is 100, respectively. As seen in Fig.3.2, $H(15C5)^+$, $K(15C5)^+$ and $K(15C5)_2{}^+$ were observed as the products. The peaks of Rb^+ and Cs^+ were also observed in Fig.3.2. They were thought to

Table 3.1: Physical properties of alkali metals and crown ether

cation	ionization potential[a] (eV)	ionic radius[b] (Å)	crown ether	cavity radius[b] (Å)
Li^+	5.39	0.76	12-crown-4	0.60–0.75
Na^+	5.14	1.02	15-crown-5	0.86–0.92
K^+	4.34	1.38	18-crown-6	1.34–1.43
Rb^+	4.18	1.52		
Cs^+	3.89	1.67		

[a]Reference [7]. [b]Reference [8]

be resulted by the contaminations in the previous experiments. The Fig.3.2 shows that 1:1 complex formations of $K(15C5)^+$ and $H(15C5)^+$, and subsequent reaction of $K(15C5)^+$ with an additional ligand to form 1:2 complex were occurred during the storage period. No other products such as $K(15C5)_n{}^+$ ($n \geq 3$) were observed.

As seen in Fig.3.2, $H(15C5)^+$ was observed with high intensity. On the other hand, Fig.3.3 and 3.4 show that little $H(15C5)^+$ were generated during the storage period. These results may suppose that the production efficiency reflect the ionization potentials of these alkali metal (Table. 3.1). Conceivable simple reaction pathways for production of $H(15C5)^+$ are given as

$$K^+ + (15C5) \longrightarrow (15C5)^+ + K \tag{3.2}$$

$$(15C5)^+ + (15C5) \longrightarrow H(15C5)^+ + (15C5)[\text{extracted H atom}]. \tag{3.3}$$

However, the intermediate product, $(15C5)^+$ was not observed. Thus the reaction

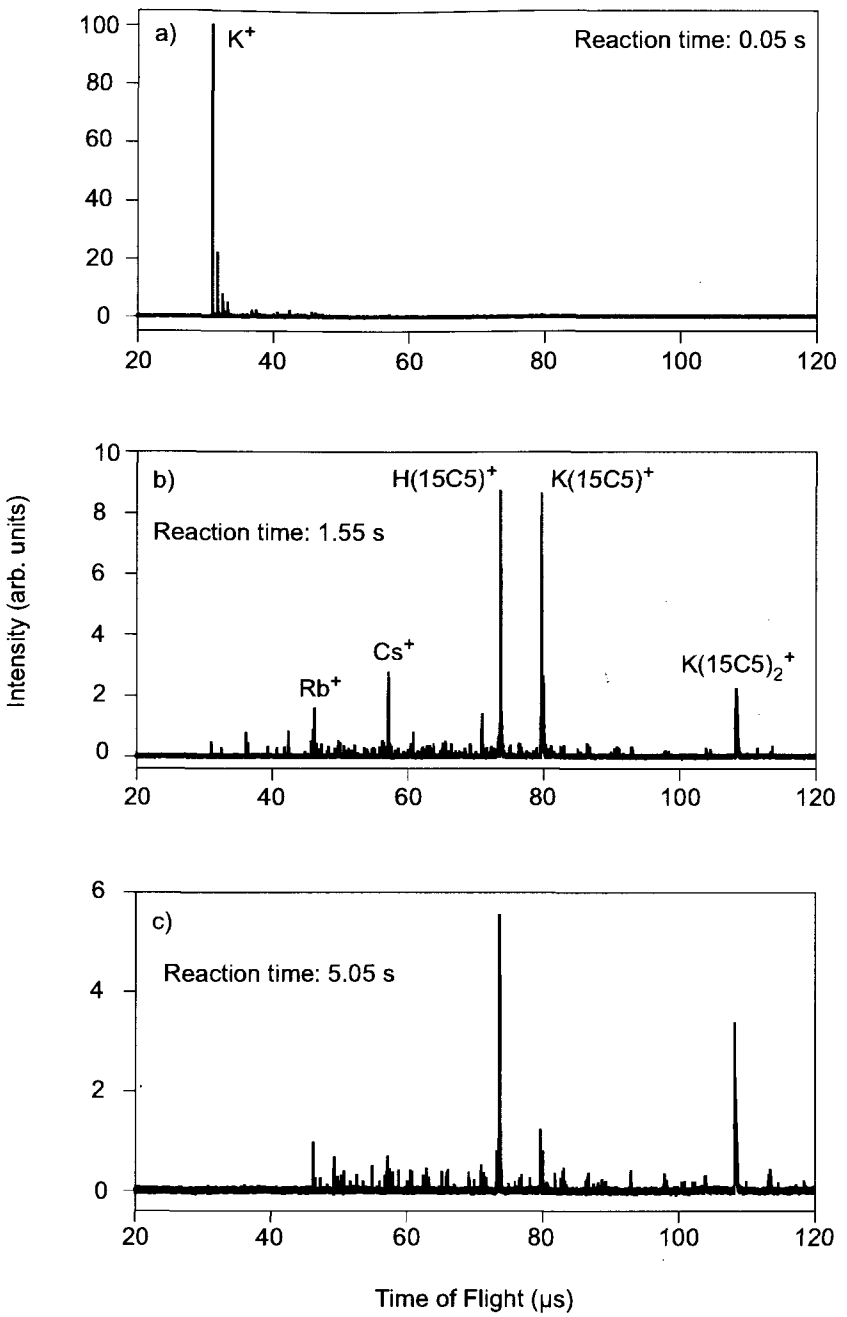

Figure 3.2: TOF spectra of the reaction products in the reactions of K^+ with 15C5 obtained with the reaction time of (a) 0.05 s, (b) 1.55 s and (c) 5.05 s.

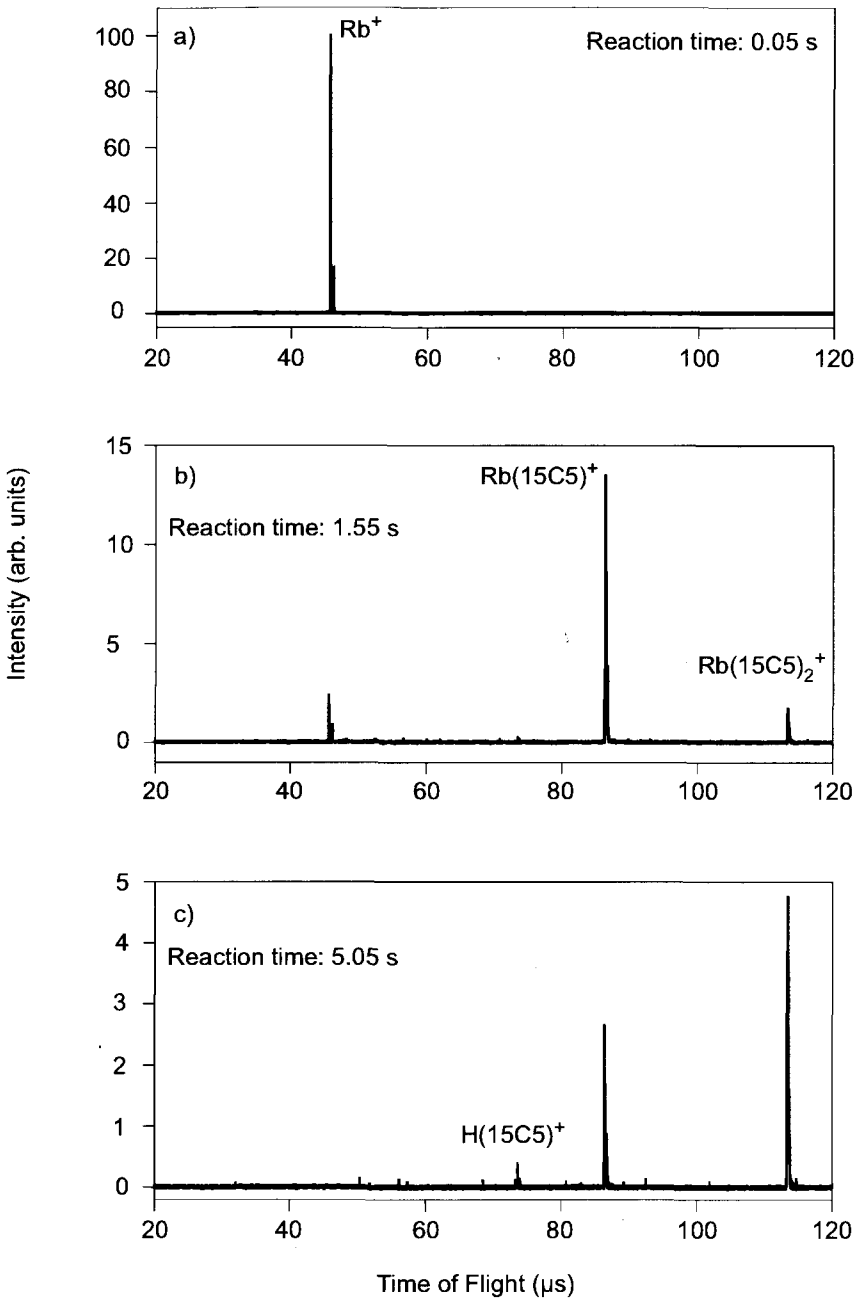

Figure 3.3: TOF spectra of the reaction products in the reactions of Rb^+ with 15C5 obtained with the reaction time of (a) 0.05 s, (b) 1.55 s and (c) 5.05 s.

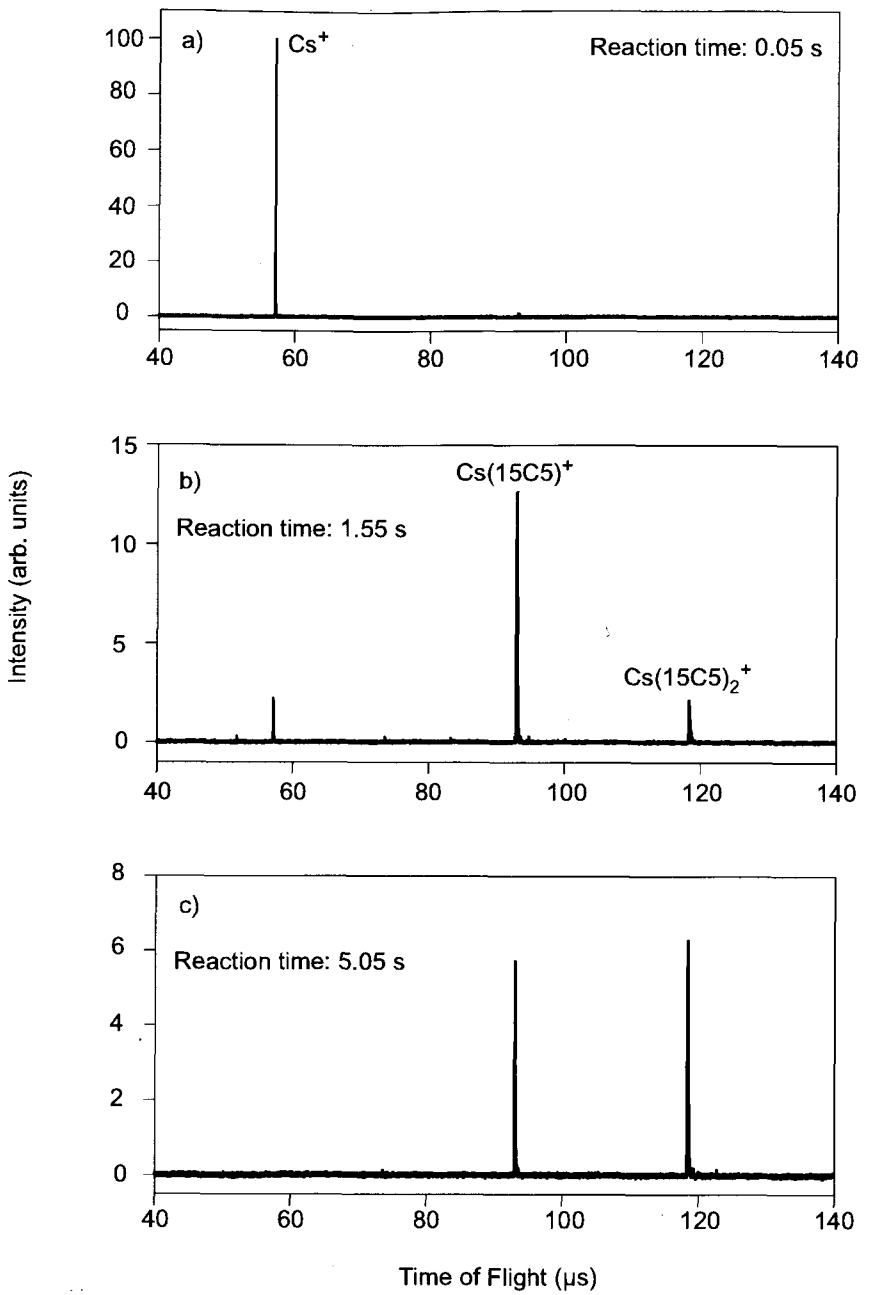

Figure 3.4: TOF spectra of the reaction products in the reactions of Cs^+ with 15C5 obtained with the reaction time of (a) 0.05 s, (b) 1.55 s and (c) 5.05 s.

mechanism for production of $H(15C5)^+$ could not be established.

In the case of Rb^+ and Cs^+, on the other hand, the consecutive reactions,

$$M^+ + (15C5) \longrightarrow M(15C5)^+ \tag{3.4}$$

and

$$M(15C5)^+ + (15C5) \longrightarrow M(15C5)_2{}^+ \tag{3.5}$$

,were observed (M indicates Rb and Cs). These reaction pathways were identical to the reactions reported previously [8].

Determining the reaction rate constants

As mentioned above, the reaction pathways for Rb^+ and Cs^+ were determined completely. Therefore, the reaction rate constants can be extracted from the obtained data. Assuming the *lifetimes* of all the stored cations was constant, let us define the branching fraction for a given product cation, f_i, as

$$f_i = I_i / \sum_i I_i \tag{3.6}$$

where I_i and $\sum I_i$ represent the intensity of the product cation, i, and the sum of the intensities of all the product cations observed, respectively. Fig.3.5 shows the branching fractions as a function of the reaction times. From the reaction formulas (3.4) and (3.5), the rate equations of the reactions can be expressed as

$$\frac{df_M}{dt} = -k_1[15C5]f_M \tag{3.7}$$

$$\frac{df_{M(15C5)}}{dt} = +k_1[15C5]f_M - k_2[15C5]f_{M(15C5)} \tag{3.8}$$

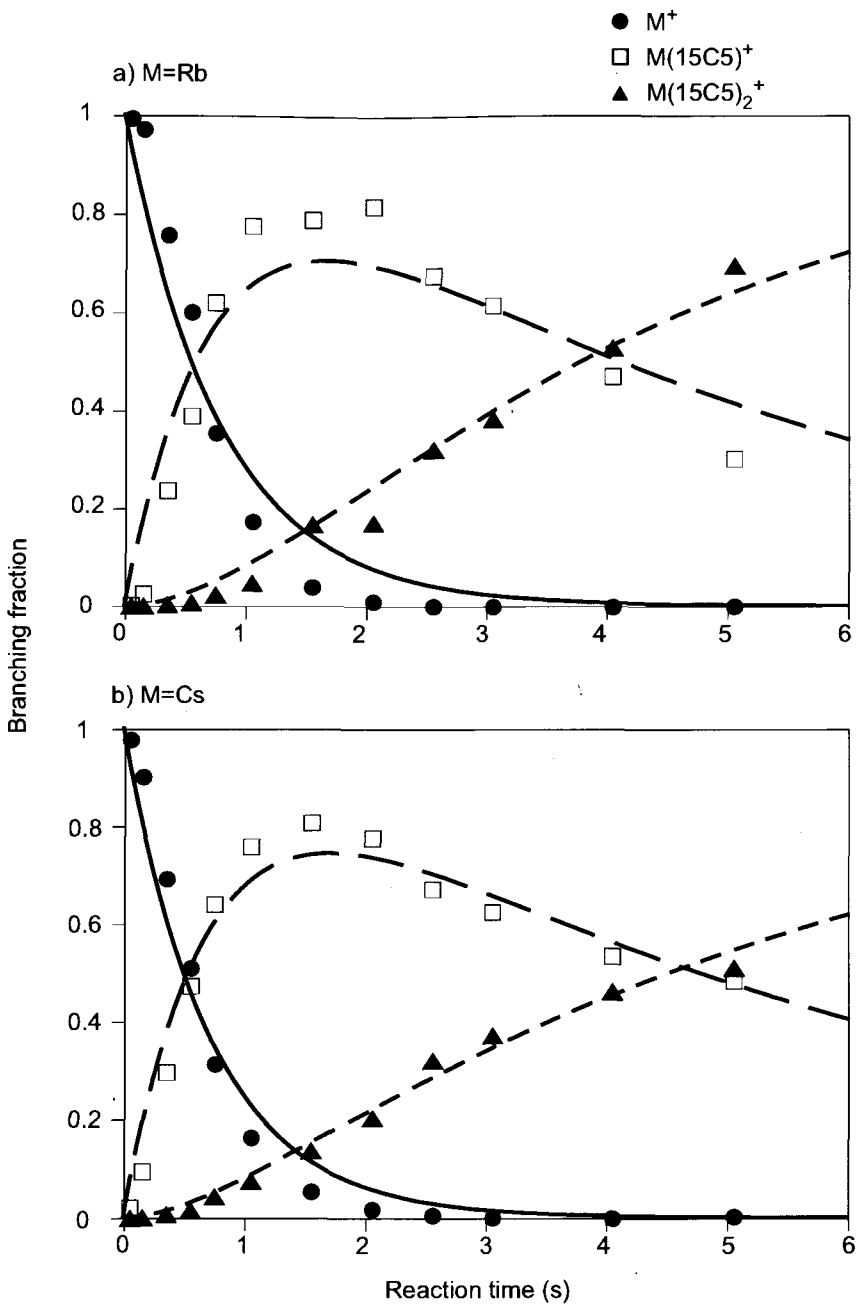

Figure 3.5: Branching fractions of the observed cations with the reaction times. The filled circles, the open squares and the filled triangles indicate the branching fractions of M^+, $M(15C5)^+$ and $M(15C5)_2^+$. (a) M = Rb and (b) M = Cs. The best fits to the data calculating the rate equations are shown as the curves (see text).

$$\frac{df_{M(15C5)_2}}{dt} = +k_2[15C5]f_{M(15C5)} \tag{3.9}$$

where k_1, k_2 and [15C5] represent the reaction rate constants of the reaction (3.4) and (3.5), and the number density of 15C5, respectively. Here, reactions (3.4) and (3.5) can be regarded as the pseudo-first-order reactions because [15C5] was kept constant during the reactions. Then substituting K_1 and K_2 for k_1[15C5] and k_2[15C5], respectively, the equations (3.7)– (3.9) can be transformed into the following forms:

$$\frac{df_M}{dt} = -K_1 f_M \tag{3.10}$$

$$\frac{df_{M(15C5)}}{dt} = +K_1 f_M - K_2 f_{M(15C5)} \tag{3.11}$$

$$\frac{df_{M(15C5)_2}}{dt} = +K_2 f_{M(15C5)}. \tag{3.12}$$

These equations are easily solved analytically as

$$f_M = \exp(-K_1 t) \tag{3.13}$$

$$f_{M(15C5)} = \frac{K_1}{K_2 - K_1}[\exp(-K_1 t) - \exp(-K_2 t)] \tag{3.14}$$

$$f_{M(15C5)_2} = 1 - \frac{1}{K_2 - K_1}[K_2 \exp(-K_1 t) - K_1 \exp(-K_2 t)]. \tag{3.15}$$

Fitting these curves to the data points, we can obtain K_1 and K_2. The curves in Fig.3.5 were fitted to the points by the general fitting function of a computer software (KaleidaGraph 3.6, Synergy Software, Pennsylvania, USA) which employs a Levenberg-Marquardt algorithm [9].

The number density of 15C5, [15C5], can be calculated by obtaining the absolute partial pressure of 15C5. In the present study, however, an ionization gauge, which is a relative pressure gauge basically, is employed. Thus the readings of

the gauge are required to be transformed into the absolute pressure. Bartmess et al. [10] have been reported that the relative sensitivities of a ionization gauge is obtained by an empirical formula as

$$R_x = 0.36\alpha + 0.30 \tag{3.16}$$

where R_x and α are the sensitivity relative to $N_2 = 1.00$ and the polarizability of the molecules. Thus the number density of 15C5 can be obtained if α for 15C5 is known. Unfortunately, however, the data of α for 15C5 have not been reported. Then even though it is a rough estimation, the polarizability of 15C5 can be calculated by a empirical method [11]. This method gives a molecular polarizability as

$$\alpha = \frac{4}{N}\left[\sum_A \xi_A\right]^2 \tag{3.17}$$

where N is the number of electrons in the molecule, and the parameter ξ_A is the *atomic hybrid component* for each atom A in a particular configuration of the molecule. The polarizability of 15C5 calculated by this method is 21.96 $Å^3$. From the equation (3.16), therefore, the relative sensitivity of the gauge is obtained as $R_x = 8.21$ and the number density of 15C5 can be calculated from the readings of the gauge.

The reaction rate constants obtained according to the above procedure are listed in Table 3.2. For further references, the rate constants obtained in another experimental condition are also listed in the table (lower column). In this experiment, helium was introduced in the vacuum chamber continuously (without using a pulsed valve), i.e. the ion/molecule reactions were occurred in the presence of

Table 3.2: Rate constants, k_1 and k_2 (10^{-10} cm^3 $molecule^{-1}$ s^{-1}), for formation of 1:1 alkali cation–15C5 complex

cation	k_1(present study) (without He pulse[a])	k_1[b]	k_1/k_1[b]	k_2	k_2[b]	k_2/k_2[b]
K^+		52.5 ± 37.9			4.51 ± 1.90	
Rb^+	8.8 ± 1.4	14.4 ± 2.6	0.6 ± 0.2	1.5 ± 0.4	2.95 ± 1.01	0.5 ± 0.2
	24 ± 4		1.7 ± 0.4	14 ± 2		4.7 ± 1.8
Cs^+	6.8 ± 0.5	11.0 ± 1.9	0.6 ± 0.1	0.9 ± 0.3	1.34 ± 0.37	0.7 ± 0.3
	17 ± 4		1.5 ± 0.5	7 ± 2		5.2 ± 2.1

[a]Experiment with continuously introducing helium (see text). [b]Reference [6].

many helium atoms. As shown in the table, the values obtained in this condition are considerable larger than those of the present experiments (with using pulsed valve). This fact indicates that helium atom act as a third-body of the reactions. Thus it can be concluded that the pulsed helium injection is essential in observation of elementary reactions. In both cases, the absolute rate constants obtained by the present study are different from those reported previously [6]. However, the tendencies of the changes in these values are in good agreement. The following are the conceivable causes of differences in these values: the uncertainties of the number density of 15C5 might be large. In present study, the absolute number density were estimated by various steps described above. These estimations are quite rough ways to calculate the pressure. To settle this problem, the method to determine the absolute pressure of the ligands inside the ion trap is required to be established. For instance, the measurements of a well-known reaction as a pressure reference with a pressure gauge which can measure the absolute pressure such as a capacitance manometer may enable to estimate the number densities of ligands more precisely. Even though some problems still remain, the relative reaction efficiencies are consistent with that obtained previously. Thus the device

can be applied to the qualitative analysis of ion/molecule reactions.

3.4 Conclusion

Using the cylindrical ion trap TOF mass spectrometer, the ion/molecule reactions of alkali metal cations, K^+, Rb^+ and Cs^+, with crown ether, 15C5, were observed. The reaction pathways of Rb^+ and Cs^+ with 15C5 were determined. These reaction pathways were identical to those reported previously. On the other hand, the reaction pathways of K^+ could not be established because of formation of $H(15C5)^+$. The reaction rate constants of Rb^+ and Cs^+ were also obtained from the data. These values showed the same tendency of those reported previously, but the absolute values were quite different. These disagreements in the values might be caused by the uncertainties of the absolute pressure inside the ion trap. The preliminary conclusion was that this apparatus can be used for qualitative analysis such as determining the reaction pathways, and that there is much room for further improvement on ability for quantitative analysis.

References

[1] M. B. More, D. Ray, and P. B. Armentrout, J. Am. Chem. Soc. **121**, 417 (1999).

[2] D. V. Dearden, Y. Liang, J. B. Nicoli, and K. A. Kellersberger, J. Mass Spectrom. **36**, 989 (2001).

[3] S. E. Hill, E. D. Glendening, and D. Feller, J. Phys. Chem. A **101**, 6125 (1997).

[4] P. B. Armentrout, Int. J. Mass Spectrom. **193**, 227 (1999).

[5] E. D. Glendening, D. Feller, and M. A. Thompson, J. Am. Chem. Soc. **116**, 10657 (1994).

[6] I. H. Chu, H. Zhang, and D. V. Dearden, J. Am. Chem. Soc. **115**, 5736 (1993).

[7] National Astronomical Observatory, editor, *Rika nenpyo (Chronological Scientific Tables)*, Maruzen, Tokyo, 1999.

[8] H. Zhang, I. H. Chu, S. Leming, and D. V. Dearden, J. Am. Chem. Soc. **113**, 7415 (1991).

[9] W. H. Press, B. P. Flannery, S. A. Teukolsky, and W. T. Vetterling, *Numerical Recipes in C*, Cambridge University Press, New York, 1988.

[10] J. E. Bartmess and R. M. Georgiadis, Vacuum **33**, 149 (1983).

[11] K. J. Miller and J. A. Savchik, J. Am. Chem. Soc. **101**, 7206 (1979).

Chapter 4

Observation of Ion/Molecule Reactions of Silver Cluster Cations with Crown Ether

4.1 Introduction

It is known that clusters react with various molecules. Their interesting aspects are dependence of reactivity on the number of atoms in the cluster. These studies has been reviewed by Knickelbein [1]. For example, Irion and Schnabel [2] have reported that Fe_4^+ shows high reactivity with ammonia in contrast to their neighboring clusters. Ichihashi et al. have reported that Ni_n^+ also exhibit size-specific reactivity with methanol [3]. The reaction products, $Ni_4(CH_3OH)^+$ and Ni_4O^+, have been observed as the reaction products in case of Ni_4^+, whereas Ni_6^+ generates only $Ni_6^+(CHOH)$. Specially, the reactivity of silver cluster is of importance

because silver is used as catalysts and in photography. Thus many investigations on the reactions of silver cluster with various small molecules, such as H_2O [4], alcohols [5] and ammonia [6], have been performed. For example, it has been reported that Ag_n^+ reacts with small molecules, such as ethene, propene, benzene, etc. [7], as

$$Ag_n^+ + L \longrightarrow Ag_nL^+ \quad (n = 1, 3, 4, 5) \tag{4.1}$$

$$Ag_n^+ + L \longrightarrow Ag_{n-1}L^+ + Ag \quad (n = 2, 4) \tag{4.2}$$

where L indicates the ligand molecule. These size-specific reactions have gained more and more attention. However, the reactions of silver cluster with relatively large molecules, such as crown ethers, have not been studied yet. The ion/molecule reaction of silver cluster cations with crown ether is an appropriate example for understanding the reactivity of cluster ions and the molecular recognition mechanism. In this chapter, the observation of the ion/molecule reactions of silver cluster cations, Ag_n^+ (n = 1, 3, 5, 7 and 9), with crown ether, 12-crown-4, and these reaction pathways are reported.

4.2 Experimental

The experimental setup has been described in detail in chapter 2. In brief, silver cluster cations, Ag_n^+ (n = 1, 3, 5, 7 and 9) were produced by xenon ions bombardment on a silver plate. The acceleration energy of the primary xenon ions was 12 keV. The secondary cluster cations were then accelerated toward the deceleration lens system. The acceleration energy of the secondary cluster cations was

1.11 keV. The ions were decelerated to 1.10 keV by the deceleration lens system. Crown ether, 12-crown-4 (036-16901, Wako Pure Chemical Industries), was introduced continuously into the vacuum chamber (chamber Y in Fig.2.5) through a leak valve. The pressure of the 12C4 was controlled so as to be kept constant during the measurements by monitoring a ionization gauge. The cluster cations introduced into the cylindrical ion trap were then confirmed and thermalized by a pulse of helium introduced by a pulsed solenoid valve. The period when the valve opens was 1.5 ms and the peak pressure of helium was ca. 5×10^{-3} Pa. The ion injection time was 100 ms. To store a specific size of the cluster cations, resonance voltage was applied to the end-cap electrode for 500 ms. After a storage period, which corresponds to a reaction time, all the cations stored in the ion trap were ejected to the TOF mass analyzer. The first- and second- stage acceleration energy of the ejected cations were 0.47 and 1.10 keV, respectively. The TOF spectra were obtained by averaging 30 mesurements on a digital oscilloscope. The operating conditions for observing the reaction of the specific size of cluster cations were as follows:

Observing the reactions of Ag^+

- the rf frequency was 950 kHz,
- the rf voltage was $500V_{0-p}$,
- the frequencies applied for the resonance ejection were 1–95 and 111–150

kHz,

- the background pressure of the vacuum chamber at which the ion trap was mounted was 6.8×10^{-4} Pa,
- the pressure of the vacuum chamber during introducing 12C4 was 8.1×10^{-4} Pa, and
- the reaction times were varied from 0 s to 1.5 s.

Observing the reactions of Ag_3^+

- the rf frequency was 600 kHz,
- the rf voltage was $600V_{0-p}$,
- the frequencies applied for the resonance ejection were 1–110 and 126–150 kHz,
- the background pressure of the vacuum chamber at which the ion trap was mounted was 6.8×10^{-4} Pa,
- the pressure of the vacuum chamber during introducing 12C4 was 8.0×10^{-4} Pa, and
- the reaction times were varied from 0 s to 7.0 s.

Observing the reactions of Ag_5^+

- the rf frequency was 600 kHz,
- the rf voltage was $600V_{0-p}$,
- the frequencies applied for the resonance ejection were 1–59 and 76–150 kHz,
- the background pressure of the vacuum chamber at which the ion trap was mounted was 7.6×10^{-4} Pa,
- the pressure of the vacuum chamber during introducing 12C4 was 8.2×10^{-4} Pa, and
- the reaction times were varied from 0 s to 9.0 s.

Observing the reactions of Ag_7^+

- the rf frequency was 600 kHz,
- the rf voltage was $600V_{0-p}$,
- the frequencies applied for the resonance ejection were 1–49 and 58–150 kHz,
- the background pressure of the vacuum chamber at which the ion trap was mounted was 7.0×10^{-4} Pa,

- the pressure of the vacuum chamber during introducing 12C4 was 8.5 × 10^{-4} Pa, and
- the reaction times were varied from 0 s to 9.0 s.

Observing the reactions of Ag_9^+

- the rf frequency was 600 kHz,
- the rf voltage was $600V_{0-p}$,
- the frequencies applied for the resonance ejection were 1–36 and 41–150 kHz,
- the background pressure of the vacuum chamber at which the ion trap was mounted was 7.0 × 10^{-4} Pa,
- the pressure of the vacuum chamber during introducing 12C4 was 8.5 × 10^{-4} Pa, and
- the reaction times were varied from 0 s to 9.0 s.

4.3 Results and Discussion

4.3.1 Reactions of Ag^+

The TOF spectra of the reaction products obtained with the reaction times of 0–1.5 s are shown in Fig.4.1. The ordinates of each figure are normalized so that

the peak hight of Ag^+ at the reaction time of 0 s is 100, respectively. The notations of (n, m) indicate that the reaction products contain n silver atoms and m 12C4 molecules.

As shown in Fig.4.1, $Ag(12C4)^+$, $Ag(12C4)_2{}^+$ and $H(12C4)^+$ were produced by the subsequent reactions. These changes in the intensities of the reaction products show a similar tendency of the reactions of alkali metal cations (see chapter 3). Thus the reaction pathways of Ag^+ with 12C4 can be estimate as follows:

$$Ag^+ + (12C4) \longrightarrow Ag(12C4)^+ \tag{4.3}$$

$$Ag(12C4)^+ + (12C4) \longrightarrow Ag(12C4)_2{}^+. \tag{4.4}$$

Silver atom cation, Ag^+, has a electronic structure of $[Kr][4d]^{10}$, while alkali metal cations have electronic structures of closed s-shell. Thus it is expected that the reaction mechanism of silver atom cation is different from that of alkali metal cations. However, marked differences of these reactions were not confirmed.

4.3.2 Reactions of $Ag_3{}^+$

The TOF spectra of the reaction products obtained with reaction times 0–5.0 s are shown in Fig.4.2. The ordinates of each figure are normalized so that the peak hight of $Ag_3{}^+$ at the reaction time of 0 s is 100, respectively.

As seen in Fig.4.2, different results from the case of the reactions of Ag^+ were obtained. First, the 3:3 complex, $Ag_3(12C4)_3{}^+$, was produced by consecutive reactions. Sharpe and Cassady [7] have reported that the similar reaction products of 3:3 complexes were generated in the case of the reactions with small molecules

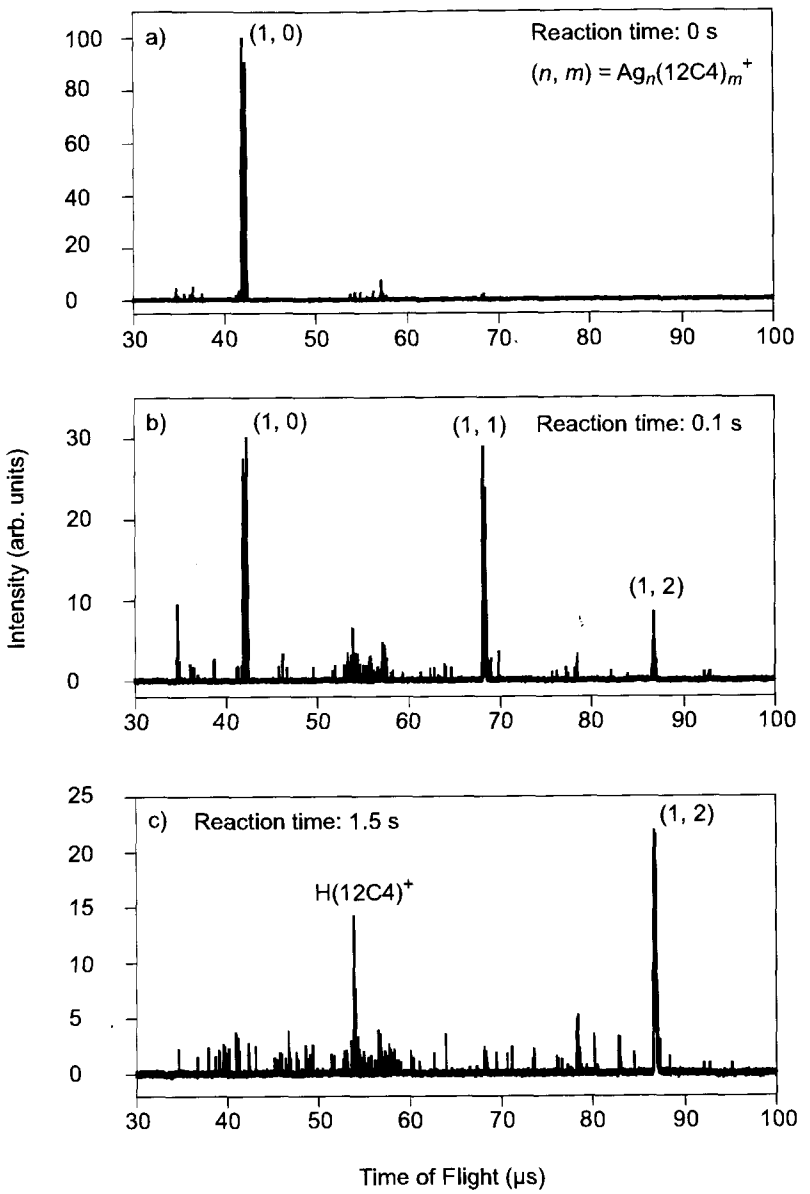

Figure 4.1: TOF spectra of the reaction products of Ag^+ with 12C4 obtained with the reaction time of (a) 0 s, (b) 0.1 s and (c) 1.5 s. All the ordinates of the spectra are normalized so that the peak hight of Ag^+ at the reaction time of 0 s is 100.

such as propene, acetone, benzene, etc. They have reported that steric requirements for such additions suggest that the most probable geometric structure of Ag_3^+ is triangular. At a rough guess, if Ag_3^+ exists in a linear geometry, it is unnatural that three ligands attach to each atom in the cluster. Theoretical and experimental studies have also indicated that Ag_3^+ exists with high stability in a triangular geometry [8, 9, 10]. The results obtained by the present study are consistent with these reports, but no conclusion can be drawn from these results until further experiments.

Second, the 1:1 and 1:2 (sandwich) complexes were also produced. On the other hand, these complexes have not been observed in the reactions with propene, acetone, benzene, etc. In the experiments under the condition that Ag_3^+ were stored in the ion trap up to 3.0 s without 12C4 (pressure in the chamber was 7.2 $\times 10^{-4}$ Pa), the spontaneous fragmentation of Ag_3^+ such as

$$Ag_3^+ \longrightarrow Ag^+ + Ag_2 \tag{4.5}$$

was not observed. Thus it can be concluded that the productions of the 1:1 and 1:2 complexes were caused by the existence of 12C4. The production of 1:1 complex might be generated by the following reaction scheme: (1) a 12C4 molecule attached to a silver atom of Ag_3^+ and generated an activated complex, (2) oxygen atoms in 12C4 attracted the positive charge in Ag_3^+ and (3) the localization of the charge caused the fragmentation to $Ag(12C4)^+$ and Ag_2. Since the intermediate, 1:1 complex, was observed with high intensity, the 1:2 complex might be

produced through the 1:1 complex. However, the minor pathway,

$$Ag_3(12C4)_2^+ \longrightarrow Ag(12C4)_2^+ + Ag_2, \tag{4.6}$$

might exist. Fig.4.3 shows the branching fractions as a function of the reaction times. From the above discussion and change with reaction time of the branching fractions, the scheme of reactions of Ag_3^+ with 12C4 is proposed as shown in Fig.4.4. As a matter of course, however, other method such as calculations of molecular structure is required to examine whether proposed scheme is acceptable or not.

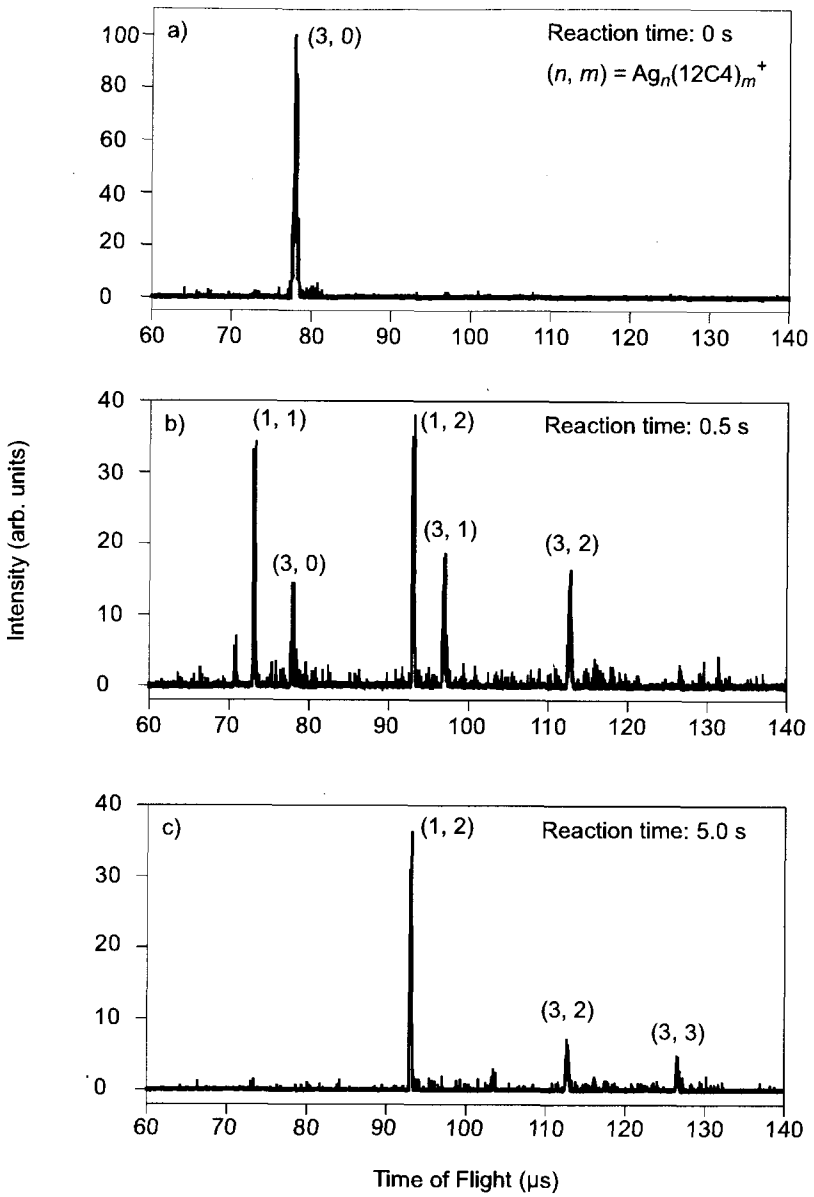

Figure 4.2: TOF spectra of the reaction products of Ag_3^+ with 12C4 obtained with the reaction time of (a) 0 s, (b) 0.5 s and (c) 5.0 s. All the ordinates of the spectra are normalized so that the peak hight of Ag_3^+ at the reaction time of 0 s is 100.

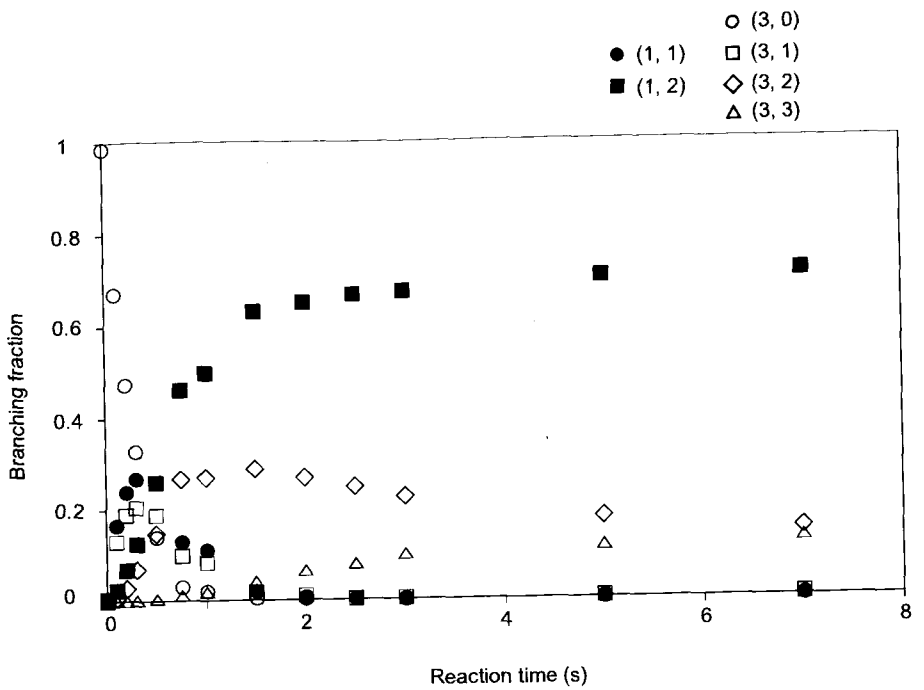

Figure 4.3: Branching fractions of the observed cations with the reaction times. The filled circles, filled squares, open circles, open squares, open diamonds and open triangles indicate the branching fractions of (1, 1), (1, 2), (3, 0), (3, 1), (3, 2) and (3, 3), respectively.

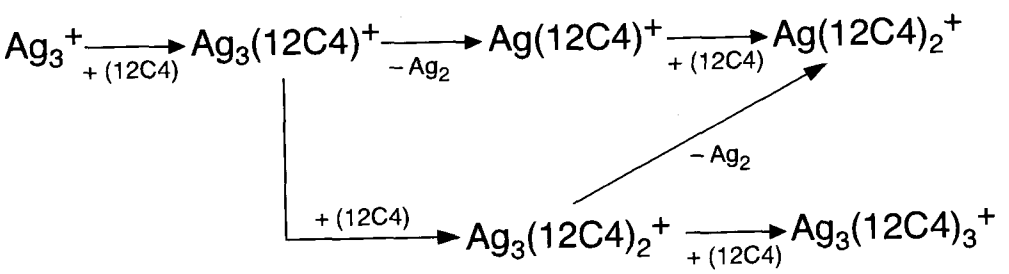

Figure 4.4: Proposed reaction scheme of Ag_3^+ with 12C4.

4.3.3 Reactions of Ag_5^+

The TOF spectra of the reaction products obtained with reaction times 0–9.0 s are shown in Fig.4.5. The ordinates of each figure are normalized so that the peak hight of Ag_5^+ at the reaction time of 0 s is 100, respectively.

As seen in Fig.4.5, it is suggested that pretty complicated reactions were occurred. Although the reactions pathways for each product were difficult to be determined, some interesting features were observed. The first attractive feature is that $Ag_3(12C4)^+$ was observed. The spontaneous fragmentation of Ag_5^+,

$$Ag_5^+ \longrightarrow Ag_3^+ + Ag_2 \tag{4.7}$$

was not observed in the preliminary experiment. Therefore, it can be suggested that the reactions as

$$Ag_5^+ + (12C4) \longrightarrow Ag_5(12C4)^+ \tag{4.8}$$

$$Ag_5(12C4)^+ \longrightarrow Ag_3(12C4)^+ + Ag_2 \tag{4.9}$$

were occurred These reaction pathways might be favorable because both of the Ag_3^+ and Ag_2 correspond to the magic numbers.

The second feature is that the complexes which have even-number silver atoms, such as $Ag_2(12C4)_2^+$ and $Ag_4(12C4)_2^+$ were produced. In the case of the reaction of Ag_3^+, these products were not observed. As seen in Fig.4.5, $Ag_2(12C4)_2^+$ and $Ag_4(12C4)_2^+$ were produced after $Ag_5(12C4)^+$ disappeared. Thus these complexes might be produced from $Ag_5(12C4)_m^+$ ($m = 2$ or 3). To examine whether $Ag_2(12C4)_2^+$ and $Ag_4(12C4)_2^+$ are intermediate products or terminal products, the observations of the reactions for longer reaction periods is required.

The third feature is that the 1:2 complex, $Ag(12C4)_2^+$, was seen to be mainly produced without intermediate formation of $Ag(12C4)^+$. There is possibility that two 12C4 molecules can attach to one silver atom in Ag_5^+ and then $Ag(12C4)_2^+$ is produced. Although it is difficult to estimate the whole reaction pathways because of complexity, the proposed pathways are shown in Fig.4.6.

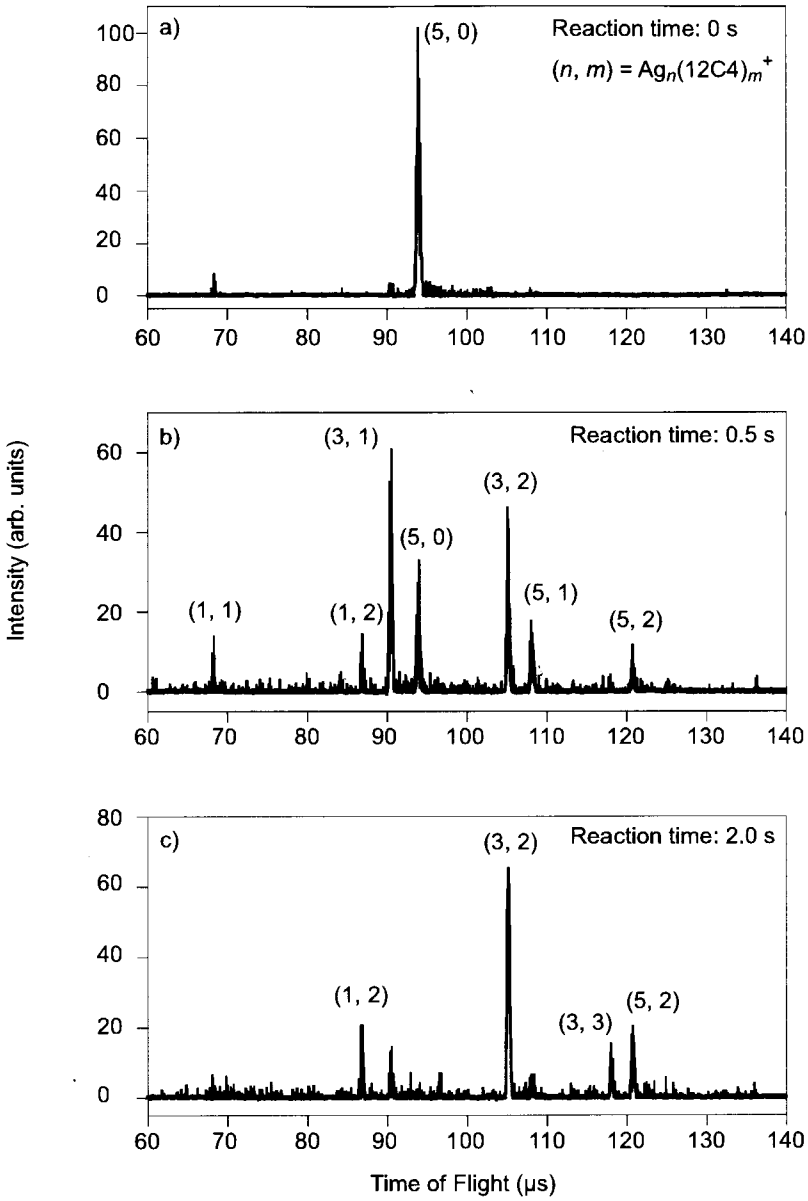
a)
(5, 0)
Reaction time: 0 s
(n, m) = Ag$_n$(12C4)$_m^+$
b)
(3, 1)
(3, 2)
(5, 0)
(5, 1)
(1, 1)
(1, 2)
(5, 2)
Reaction time: 0.5 s
c)
(3, 2)
Reaction time: 2.0 s
(1, 2)
(5, 2)
(3, 3)
Intensity (arb. units)
Time of Flight (μs)

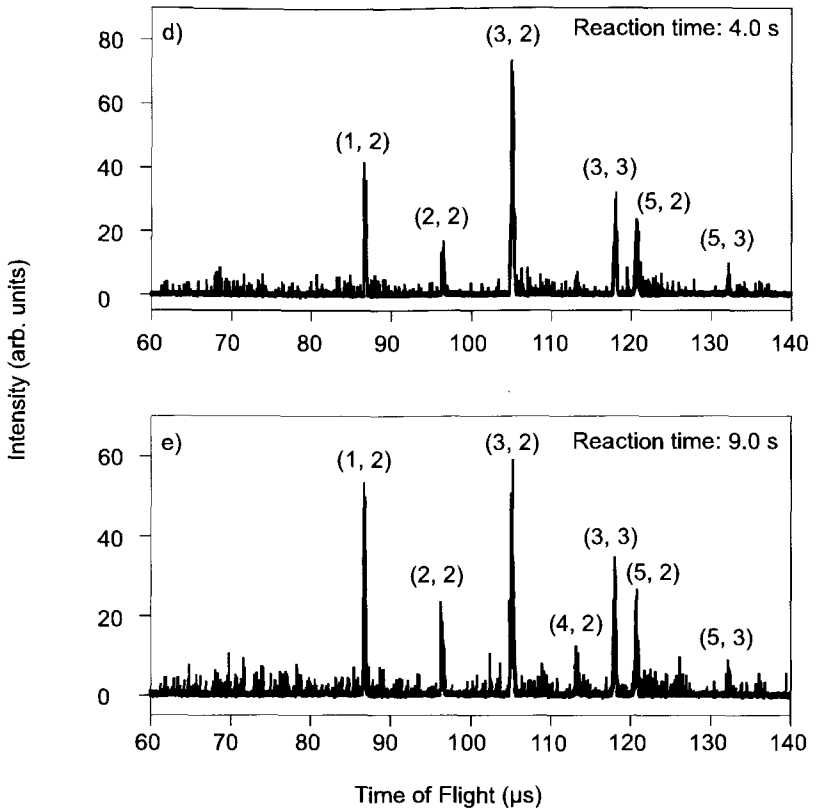

Figure 4.5: TOF spectra of the reaction products of Ag_5^+ with 12C4 obtained with the reaction time of (a) 0 s, (b) 0.5 s and (c) 2.0 s, (d) 4.0 s and (e) 9.0 s. All the ordinates of the spectra are normalized so that the peak hight of Ag_5^+ at the reaction time of 0 s is 100.

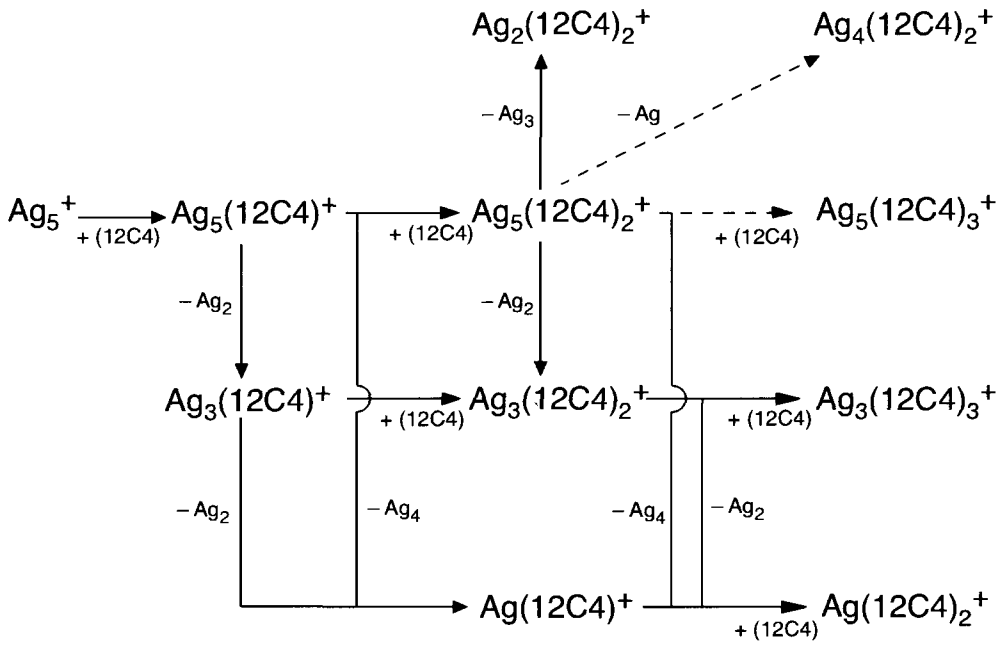

Figure 4.6: Proposed reaction scheme of Ag_5^+ with 12C4.

4.3.4 Reactions of Ag_7^+ and Ag_9^+

The TOF spectra of the reaction products obtained with reaction times 0–5.0 s are shown in Fig.4.7 and Fig.4.8. The ordinates of each figure are normalized so that the peak hight of Ag_7^+ and Ag_9^+ at the reaction time of 0 s is 100, respectively.

As seen in Fig.4.7 and Fig.4.8, similar tendencies were showed in the both cases. $Ag(12C4)^+$, $Ag(12C4)_2^+$, $Ag_n(12C4)^+$ and $Ag_n(12C4)_2^+$ ($n = 7$ and 9) were mainly observed as the reaction products in each case. $Ag_n(12C4)_m^+$ ($m \geq 3$) were little observed. This might be due to decreasing cation charge densities or delocalization of positive charge at the larger clusters such as $n = 7$ and 9. Namely, for the third 12C4 molecule, effective cation charge may be too little to

form n:3 complex because of the large size of the cluster and the delocalization of the charge in a small area by two 12C4 molecules.

Contrary to the case of Ag_5^+, $Ag_3(12C4)_m^+$ (m = 1–3) were not observed. In the case of Ag_7^+ and Ag_9^+, dissociated neutral, Ag_4 and Ag_6, produced by the production of $Ag_3(12C4)_m^+$ do not correspond to the magic numbers. These facts suggest that the productions of $Ag_3(12C4)_m^+$ from $Ag_5(12C4)_m^+$ is exceptionally favorable process.

Another feature is that 1:2 complex, $Ag(12C4)_2^+$, was seen to be mainly produced without intermediate formation of $Ag(12C4)^+$ as seen in the case of Ag_5^+. The fact indicate that the positive charge in the cluster was strongly localized by 12C4 molecule and then the localization caused dissociation of the cluster. Fig.4.9 shows the branching fractions as a function of the reaction times. In case of Ag_7^+ and Ag_9^+, it is somewhat easy to estimate the reaction pathways because of less product species. From the above discussion and Fig.4.9, the reaction pathways of Ag_7^+ and Ag_9^+ can be proposed as in Fig.4.10.

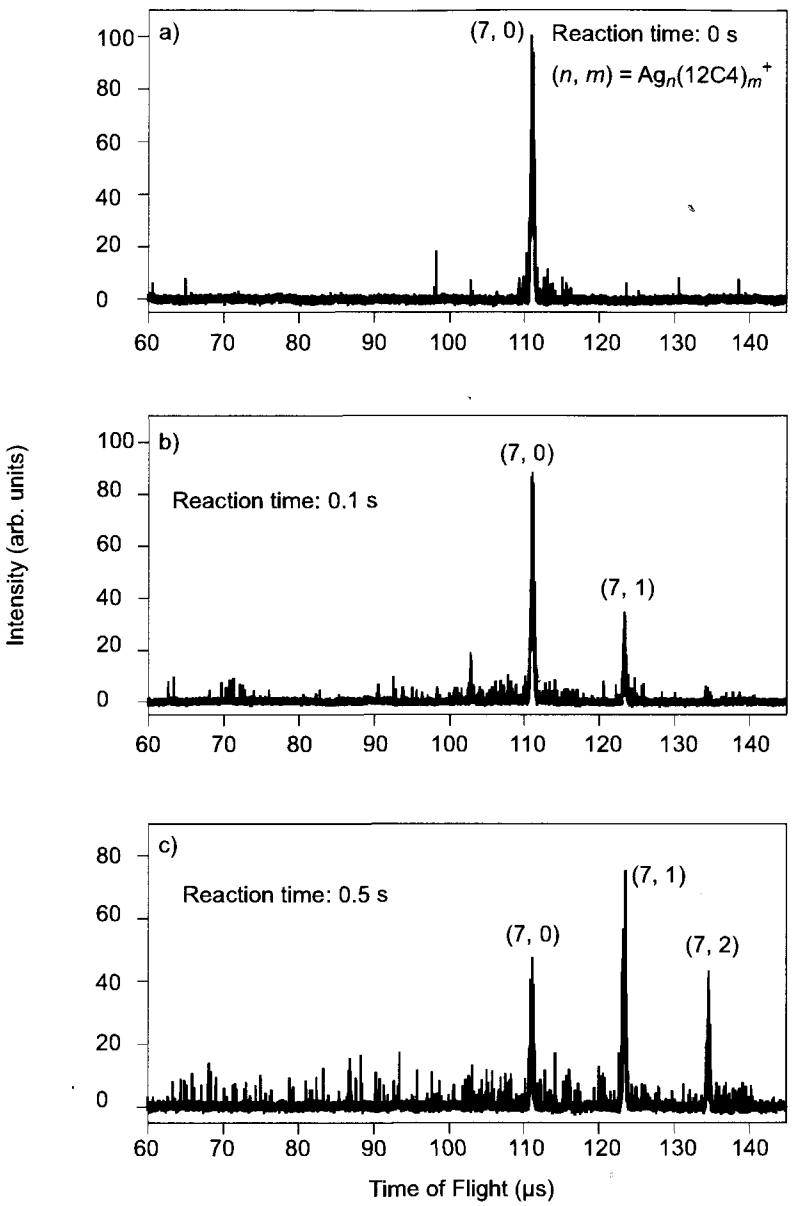
a)
(7, 0)
Reaction time: 0 s
(n, m) = Ag$_n$(12C4)$_m^+$
b)
Reaction time: 0.1 s
(7, 0)
(7, 1)
c)
Reaction time: 0.5 s
(7, 0)
(7, 1)
(7, 2)
Intensity (arb. units)
Time of Flight (μs)

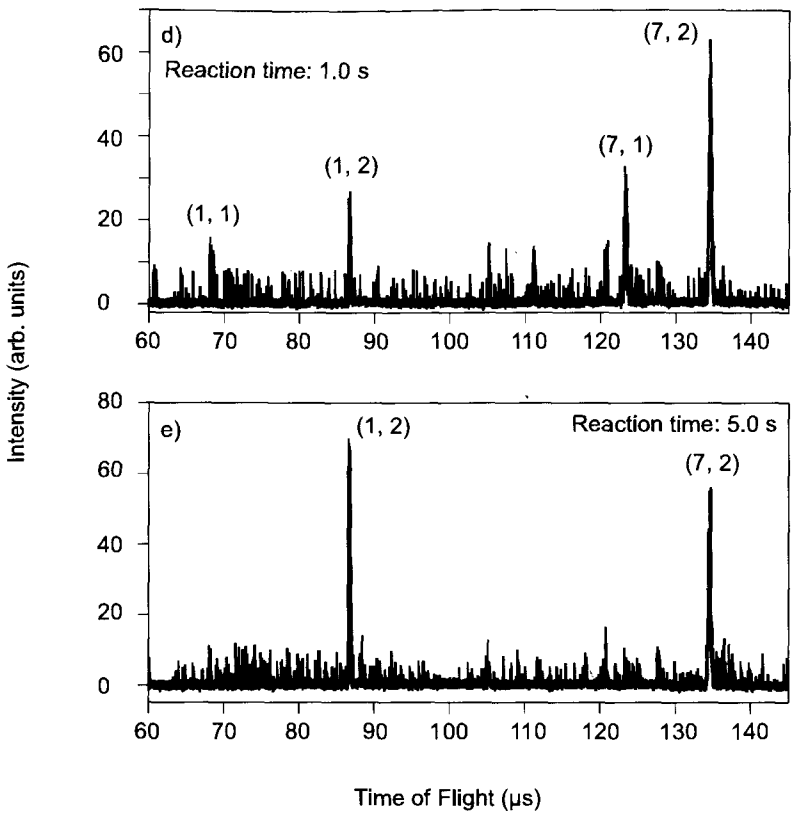

Figure 4.7: TOF spectra of the reaction products of Ag_7^+ with 12C4 obtained with the reaction time of (a) 0 s, (b) 0.1 s, (c) 0.5 s, (d) 1.0 s and (e) 5.0 s. All the ordinates of the spectra are normalized so that the peak hight of Ag_7^+ at the reaction time of 0 s is 100.

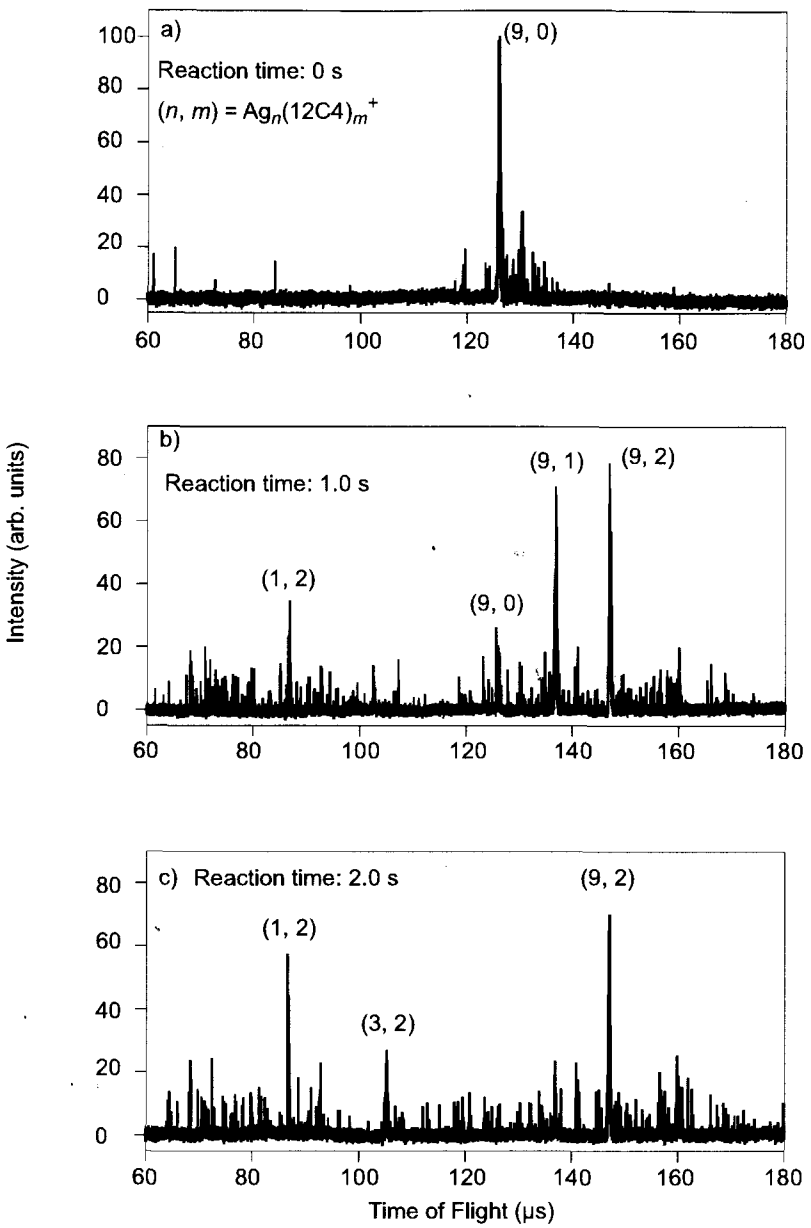
a)
Reaction time: 0 s
(n, m) = Ag$_n$(12C4)$_m^+$
(9, 0)
b)
Reaction time: 1.0 s
(1, 2)
(9, 0)
(9, 1)
(9, 2)
c) Reaction time: 2.0 s
(1, 2)
(3, 2)
(9, 2)
Intensity (arb. units)
Time of Flight (μs)

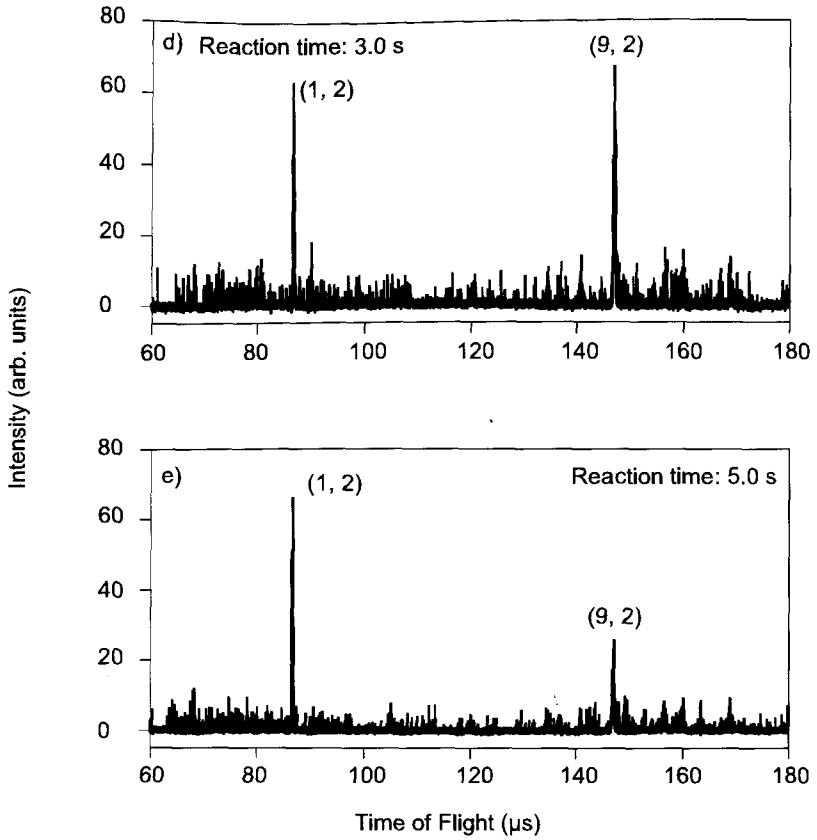

Figure 4.8: TOF spectra of the reaction products of Ag_9^+ with 12C4 obtained with the reaction time of (a) 0 s, (b) 1.0 s, (c) 2.0 s, (d) 3.0 s and (e) 5.0 s. All the ordinates of the spectra are normalized so that the peak hight of Ag_9^+ at the reaction time of 0 s is 100.

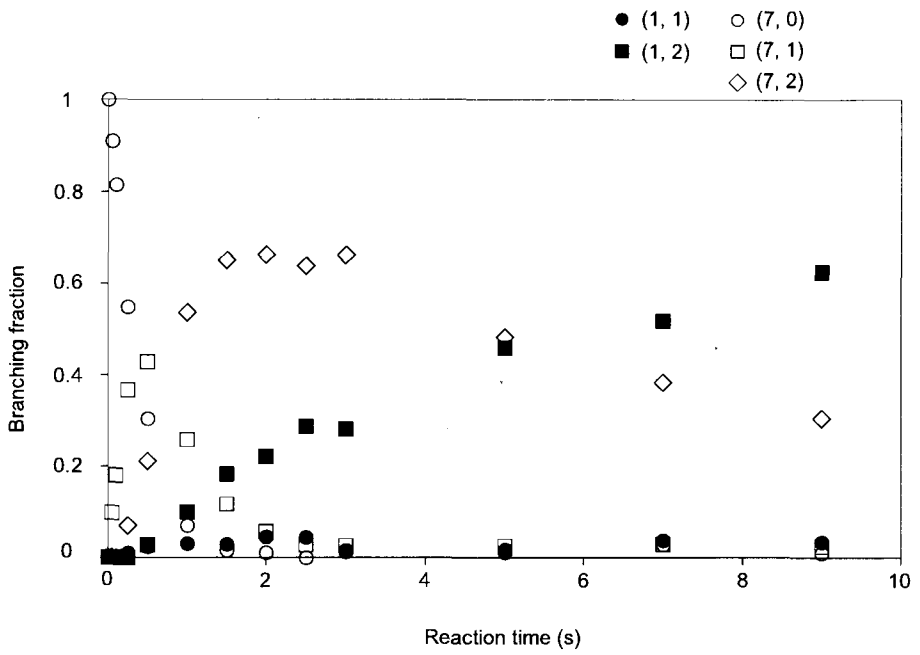

Figure 4.9: Branching fractions of the observed cations with the reaction times. The filled circles, filled squares, open circles, open squares and open diamonds indicate the branching fractions of (1, 1), (1, 2), (7, 0), (7, 1) and (7, 2), respectively.

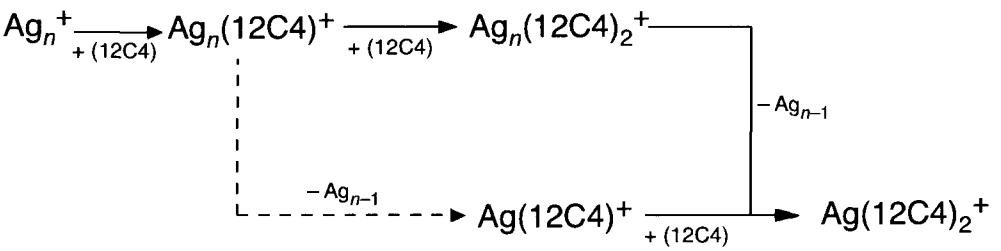

Figure 4.10: Proposed reaction scheme of Ag_n^+ ($n = 7$ and 9) with 12C4.

4.4 Conclusion

Using the cylindrical ion trap TOF mass spectrometer, the ion/molecule reactions of silver cluster cations, Ag_n^+ (n = 1, 3, 5, 7 and 9), with 12C4 were investigated. The reaction pathways of these reactions were proposed. In the case of Ag^+, the reactions which are similar to those of alkali metal cations occurred. In the case of Ag_3^+, $Ag_3(12C4)_3^+$ was observed as a reaction product. Additionally, $Ag(12C4)^+$ was observed as the reaction product from $Ag_3(12C4)^+$. This type of reaction have not been reported.

In the case of Ag_5^+, rather complicated reactions occurred. The main reaction products, $Ag_3(12C4)_m^+$ from $Ag_5(12C4)_m^+$ (m = 1 and 2) and the minor products, $Ag_5(12C4)_3^+$ were observed. The reactions for production of $Ag_3(12C4)_m^+$ are attributed to the fact that the both abstracted Ag_3^+ and Ag_2 correspond to magic number.

In the cases of Ag_7^+ and Ag_9^+, similar reactions were observed. The reaction products, $Ag(12C4)_2^+$, was mainly produced through intermediate $Ag_n(12C4)_2^+$ (n = 7 and 9). These results indicate that the production of $Ag(12C4)_2^+$ from $Ag_n(12C4)_2^+$ are favorable process, which is similar to the case of Ag_3^+. Contrary to the case of Ag_5^+, $Ag_3(12C4)_m^+$ was not observed. These results suggest that the production of $Ag_3(12C4)_m^+$ from $Ag_5(12C4)_m^+$ (m = 1 and 2) is exceptionally favorable process.

References

[1] M. B. Knickelbein, Annu. Rev. Phys. Chem. **50**, 79 (1999).

[2] M. P. Irion and P. Schnabel, J. Phys. Chem. **95**, 10596 (1991).

[3] M. Ichihashi, T. Hanmura, R. T. Yadav, and T. Kondow, J. Phys. Chem. A **104**, 11885 (2000).

[4] H. Koizumi, M. Larson, F. Muntean, and P. B. Armentrout, Int. J. Mass Spectrom. **228**, 221 (2003).

[5] P. Sharpe, J. M. Campbell, and C. J. Cassady, Organometallics **13**, 3077 (1994).

[6] M. P. Irion, P. Schnabel, and A. Selinger, Ber. Bunsenges. Phys. Chem. **94**, 1291 (1990).

[7] P. Sharpe and C. J. Cassady, Chem. Phys. Lett. **191**, 111 (1992).

[8] P. Weis, T. Bierweiler, S. Gilb, and M. M. Kappes, Chem. Phys. Lett. **355**, 355 (2002).

[9] J. Yoon, K. S. Kim, and K. K. Baeck, J. Chem. Phys. **112**, 9335 (2000).

[10] H. Basch, J. Am. Chem. Soc. **103**, 4657 (1981).

Acknowledgements

I would like to express my sincere appreciation to Professor Itsuo Katakuse, under whose guidance the work was conducted and completed. I also express my gratitude to Dr. Morio Ishihara for many useful suggestions and advice. I express my heartfelt thanks to Dr. Michisato Toyoda for introducing me to the field of mass spectrometry and many useful suggestions. I express my warm appreciation to Mr. Hiroyuki Ito for helpful suggestions. I greatly acknowledge to Mr. Toshio Ichihara and Mr. Kazurou Nakano for many technical supports.

I express thanks to Dr. Kenichi Iwamoto of Osaka Prefecture University for many useful suggestions. I express my gratitude to Professor Masahiro Kimura of Kochi University of Technology for his encouragement and suggestions. I express my warm appreciation to Dr. Takae Takeuchi of Nara Women's University for helpful suggestions.

Finally, I appreciate to my colleagues. Especially, I am indebted to Mr. Daisuke Okumura and Mr. Masaru Nishiguchi for helpful discussions.